DEOXYGENATION OF BIOMASS OXYGENATES TO HYDROCARBON FUELS VIA DIRECT METHANE INTERVENTION

A Dissertation

by

DUMINDA ANURADH GUNAWARDENA

Submitted to the Office of Graduate and Professional Studies of
Texas A&M University
in partial fulfillment of the requirements for the degree of

DOCTOR OF PHILOSOPHY

Chair of Committee:	Sandun D. Fernando
Committee Members:	Ronald E. Lacy
	Alex Thomasson
	Abraham Clearfield
Head of Department:	Stephen W. Searcy

December 2014

Major Subject: Biological and Agricultural Engineering

ABSTRACT

One of the most pressing technical challenges in the production of biofuels from biomass is the unavailability of economical processes to remove 30-45% (w/w) of the oxygen that is present in biomass-derived oxygenates. The most promising technology that exists today is hydrodeoxygenation, which requires approximately 132 lb of hydrogen to deoxygenate every ton of biomass. The cost associated with the use of H_2 for hydrodeoxygenation has an adverse effect on the economics of biofuels and the long-term sustainability of biorefineries. Therefore, there is a need for an economical and sustainable mechanism for removing oxygen (deoxygenation) from biorenewable feedstock to produce hydrocarbons.

The overall objective of this study was to determine whether methane could be used as a direct hydrogen donor (instead of gaseous hydrogen) to deoxygenate biomass-derived oxygenates to produce hydrocarbons over an appropriate metal supported ZSM-5 catalyst. To test this idea and to elucidate the reaction characteristics, six separate studies were conducted, i.e., the proof of the concept, a thermodynamic study, a catalyst screening study, a chemical kinetics study, a catalyst deactivation study, and an economic analysis.

It was observed that three separate reaction schemes involving methane and glucose pyrolysis vapor took place, depending on the type of metal or oxide used. The thermodynamic equilibrium analysis provided valuable insights concerning the theoretical limits of the desired products when a substrate reacted under a given set of

conditions. At high temperature, it was observed that CO and H_2 dominate the equilibrium mixture, with mole fractions of 0.597 and 0.587, respectively. The catalyst screening study indicated that the highest aromatic selectivity, i.e., 5.93%, was obtained for 5% Ga/ZSM-5 and that the highest furan conversion, i.e., 93.3% was obtained for5% Ni/ZSM-5. The chemical kinetics study indicated that the deoxygenation of furan was a first-order reaction with respect to the furan concentration and a second-order reaction with respect to methane concentration. The catalyst deactivation study indicated that at 500 ^{o}C coke formation reached a steady state with a coke yield of 8.0 %(w/w). The characterization of bio-oil derived from two types of feedstock, i.e., cellulose and sorghum, indicated that the presence of methane had a significant impact on reducing the oxygen content of bio-oil and increasing its heating value.

DEDICATION

To all of the brilliant scientists and engineers who have made the world a better place to live.

ACKNOWLEDGMENTS

I thank my committee chair, Dr. Fernando, and my committee members, Dr. Lacy, Dr. Thomasson, and Dr. Clearfield, for their guidance and support throughout the course of this research.

Thanks also to my friends and colleagues for making my time at Texas A&M University a great experience. I also want to extend my gratitude to the National Science Foundation, which provided the financial support to conduct this research.

I offer my sincere thanks to my parents Maulikantha Gunawardena and Kumarajeeva Gunawardena and my brother Shane Gunawardena for their encouragement and love.

TABLE OF CONTENTS

Page

LIST OF FIGURES

Page

LIST OF TABLES

Page

CHAPTER I

INTRODUCTION AND LITERATURE REVIEW*

Concerning crude oil, dwindling reserves, uncertain economics, and environmental concerns have instigated an extensive search for alternatives for producing transportation fuels. Renewable biomass resources are a potential alternative to petroleum and coal for the production of fuel and chemicals [1-4]. Biomass has been closely scrutinized as an alternative raw material to produce transport fuels and chemicals that are identical to those produced using petroleum resources [5, 6]. The increasing and efficient use of bio-fuels has greatly reduced the net CO_2 emissions into the atmosphere [6-8]; in addition, these fuels can be considered to be 'clean' since they contain negligible amounts of sulfur and nitrogen. The CO_2 emissions are considered to be neutral since CO_2 is recycled by trees, plants, and other vegetation through photosynthesis [9]. Liquid bio-fuels, such as biomass-derived ethanol and biodiesel based on vegetable oil and animal fat, are good substitutes for conventional petroleum fuels. However, they can meet only a limited portion of the world's ever-increasing demand for energy. In this context, lignocellulosic feedstock is the best hope for biomass-based energy production [10, 11].

Figure 1 shows several different ways that energy generation from biomass has been explored. . Physico-chemical conversion, mainly biodiesel production, is one of the latest studies in the conversion of biomass to energy. Primarily, this technology targets

* Printed in part with permission from Gunawardena, D.A. and S.D. Fernando, *Methods and Applications of Deoxygenation for the Conversion of Biomass to Petrochemical Products*, in *Biomass Now - Cultivation and Utilization*, M.D. Matovic, Editor. 2013, InTech. p. 273-298. Copyright 2014 InTech.

the conversion of the triglyceride fraction of biomass into fatty acid methyl esters (commonly known as biodiesel). Biochemical conversion encompasses the conversion of biomass to alcohols, primarily ethanol, and it has been studied extensively using corn as a feedstock.

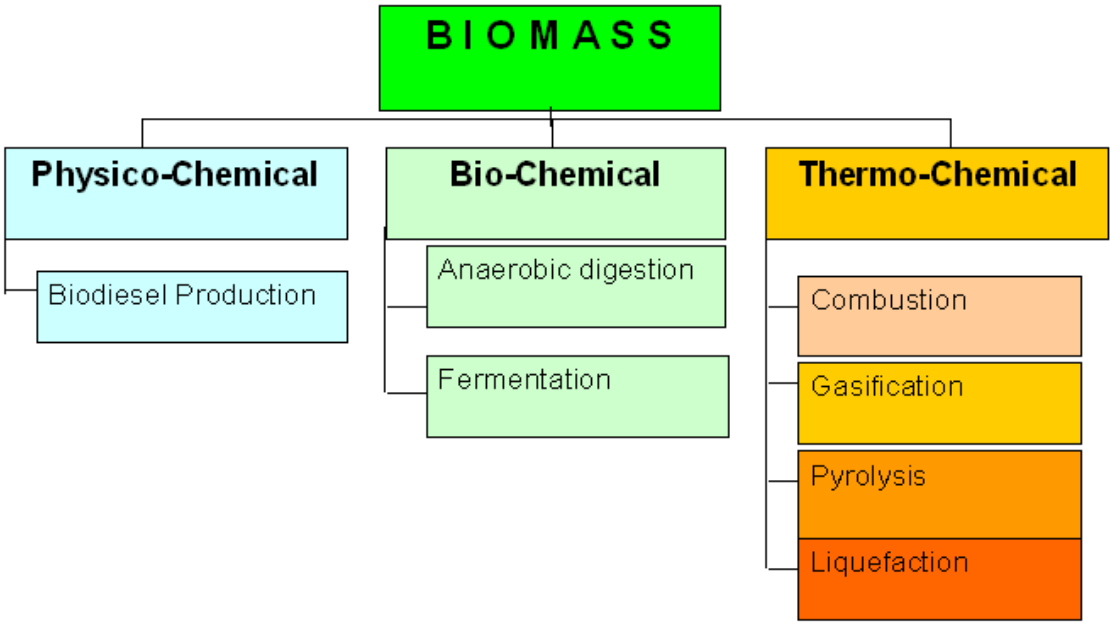

Figure 1. Different processes of biomass conversion

Among the alternative pathways, thermochemical conversion is considered to be a key process in that it primarily uses heat to induce chemical conversions and produce energetically-useful end products. Gasification is the most mature of these technologies, and it converts biomass to a mixture of gases, called synthesis gas (or syngas), which primarily consists of H_2, CO, CO_2, and CH_4. High pressure liquefaction and fast pyrolysis are primarily designed to produce a mixture of liquid products collectively

referred to as pyrolytic oil (sometimes called py-oil or bio-oil). The production of pyrolytic oil with the intention of converting it a product similar to or compatible with petroleum crude has been of interest for nearly 50 years. The challenge has been the effective removal of functional groups, mainly oxygenated groups, to produce liquid hydrocarbons.

As stated earlier, the conversion of biomass products that are compatible with the existing petroleum refinery infrastructure is an important goal for two reasons. First, fuels and chemicals can be produced that are identical to or compatible with petroleum-based products, i.e., gasoline, diesel fuel, and jet fuel. Second, the use of the existing fuel production and distribution infrastructure would reduce the overall cost of bio-fuels, thereby helping to ensure the long-term sustainability of biomass-to-fuel conversion technologies.

Thermochemical conversion of biomass

The formation of glucose by photosynthesis can be considered the workhorse of cellulosic plant matter. Glucose is the simplest building block of the cellulose and hemicelluloses that account for nearly 80% of the composition of plants. The reaction of photosynthesis (Equation 1) is thermodynamically not favorable, i.e., it is not a spontaneous reaction. The reverse reaction, which is a combustion reaction, is thermodynamically spontaneous. Similarly, gasification, pyrolysis, and liquefaction are all thermodynamically favorable reactions, but these processes must occur at higher temperatures in order to circumvent the kinetic energy barrier.

$$6CO_2 + 6H_2O \longleftrightarrow C_6H_{12}O_6 + 6O_2 \quad (1)$$

Generally, biomass contains 30-40% w/w of oxygen with a H/C molar ratio of 1.20-1.43 and a specific heat value in the range of 16-19 MJ/kg [12]. Energy generation by the combustion of biomass can be considered as the oldest method that mankind has used over many centuries [13]. However, the increasing demand for transport fuels has led to the development of the other thermochemical processes mentioned in Figure 1. Therefore, greater interest has been focused on processes that involve the conversion of biomass into liquid products [12]. The fuel shortages that occurred during World War II motivated the development of gasifiers that could make fuel for motor vehicles from charcoal or wood.

Table 1. Chemical compositions of different fuels

Chemical composition	Petroleum crude	Coal-derived naphtha	Bio-oil from	
			liquefaction	pyrolysis
Carbon %	85.2	85.2	74.8	45.3
Hydrogen %	12.8	9.6	8	7.5
H/C	1.8	1.4	1.3	2
Sulphur %	1.8	0.1	<0.1	<0.1
Nitrogen	0.1	0.5	<0.1	<0.1
Oxygen	0.1	4.7	16.6	46.9

Gaseous products (mainly CO and H_2, the mixture of which is called synthesis gas) produced by the gasification of biomass can be used directly in an internal combustion engine. However, instead of using synthesis gas directly as a fuel, a method known as the Fischer-Tropsch (FT) process was developed to convert synthesis gas to liquid fuels, which are commonly known as syncrude [13, 14]. The Fischer-Tropsch process is known to be an energy-intensive process, so it is not considered to be an

economical alternative to the petroleum refinery process. However, research is still in progress to improve the FT process to make syncrude more economical [15, 16].

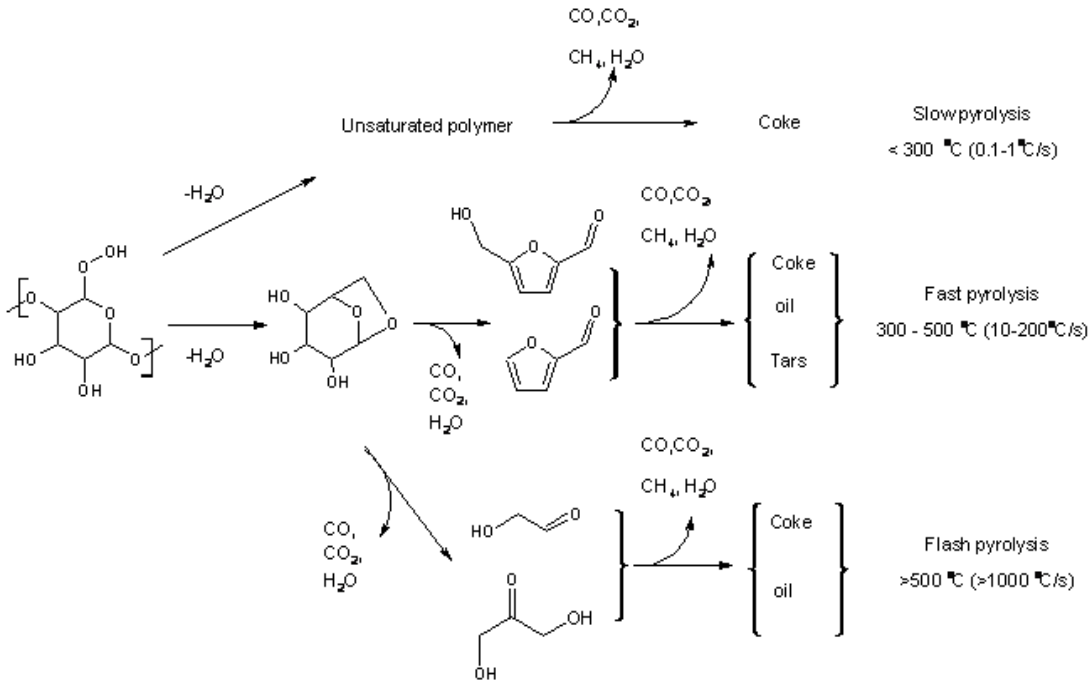

Figure 2. Reaction scheme for the pyrolysis of cellulose [17]

Pyrolysis and liquefaction are two closely-related routes for producing liquids (i.e., bio-oil or bio-crude) that are potential alternatives for petroleum crude. The composition information given in Table (1) indicates that bio-oil from pyrolysis has a higher oxygen content than it is from liquefaction [18, 19]. Although the term 'bio-oil' is not accepted universally, it generally refers to a highly-oxygenated liquid product from a pyrolysis reactor, while the term 'bio-crude' is used to represent a more deoxygenated liquid product. Bio-oil and bio-crude are mainly produced via the fast pyrolysis of biomass in the absence of oxygen at atmospheric pressure. Several types of reactors have

been designed and used for the fast-pyrolysis process, including ablative, entrained flow, rotating core, circulating fluidized bed, and deep-bubbling, fluidized-bed reactors [20]. The temperature at which the thermal scission of biomass material, such as cellulose, hemicellulose, and lignin, takes place is in the range of 450 - 550 °C. Figure 2 shows a proposed reaction pathway for the pyrolysis of cellulose. In fast pyrolysis, a very high heating rate (10-200 C^{o}/s) is used at a short residence time of the gas [21]. According to some kinetic studies conducted for different biomass materials, the frequency factor for pyrolysis varies by orders of magnitude in the range of 10^{9} - 10^{11}. This is an indication of how fast the reaction occurs [22]. Fast pyrolysis is an effective biomass conversion technology with liquid yields as high as 70 - 80%.

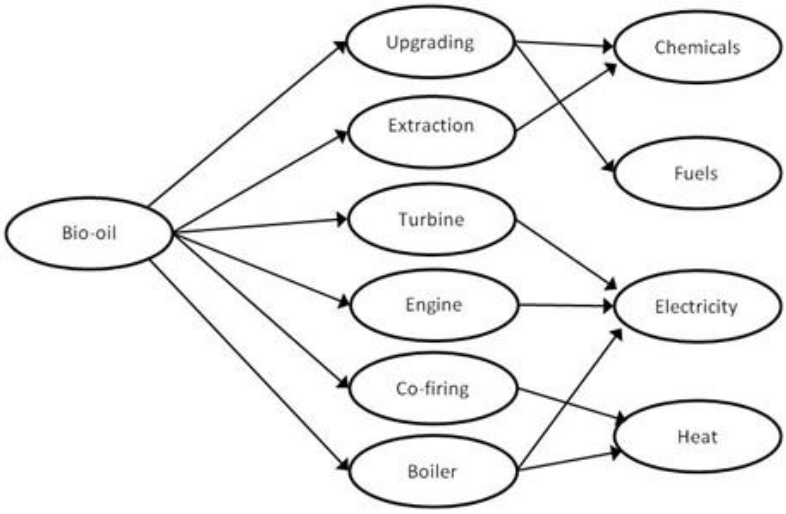

Figure 3. Industrial use of bio-oil

The overall biomass pyrolysis process can be represented by Equation (2), which is an empirical stoichiometric equation. The high fuel-to-feed ratios can be regarded as

an attractive feature of biomass pyrolysis to compete with non-renewable fossil fuel resources, which, according to some predictions, will be depleted in the next century [23].

$$CH_{1.46}O_{0.67} \longrightarrow 0.71CH_{1.98}O_{0.76} + 0.21CH_{0.1}O_{0.15} + 0.08CH_{0.44}O_{1.23} \quad (2)$$

Figure 3 shows that bio-oil, which is substantially different from petroleum crude due to the presence of high concentrations of oxygenates, already has been tested in furnaces, gas turbines [24], space heaters, and boilers [25]. Although bio-crude has the potential for use as a substitute for crude oil, some problems have been reported when it was used in industrial applications, e.g., blocking of filters by high levels of char particles, pumping issues due to high viscosity, and corrosion due to the low pH [26].

Liquefaction is another approach that can be used to produce bio-oils. Even though the concept of oil production using biomass in hot water was developed in the early 1920, a more robust and effective method did not become available until the Pittsburg Energy Research Center (PERC) demonstrated its method at the Albany Biomass Liquefaction Facility in Oregon, USA. Detailed information on this method can be found elsewhere [27]. Table (1) shows that the quality of the bio-oil from the liquefaction process was reported to be superior to that obtained from pyrolysis. The liquefaction of biomass using supercritical methods is a technique that has been investigated recently. The yield of bio-oil using supercritical methods can be as high as 95%, whereas yields in pyrolysis processes are in the range of only 50 - 60%.

Deoxygenation process and existing technologies

Pyrolysis products are highly variable and depend heavily on the type of biomass. Highly-fibrous biomass, which contains significant amounts of lignin, has been reported to be the most effective for the production of bio-oil that consists of various oxygenated aliphatic and aromatic hydrocarbons [28, 29]. Oxygenated compounds, such as aldehydes, alcohols, ketones, and carboxylic acids, are found in varying degrees in bio-oil. Figure 4 shows a typical distribution of the pyrolysis products, with large quantities of ketones, carboxylic acids, and aldehydes [30].

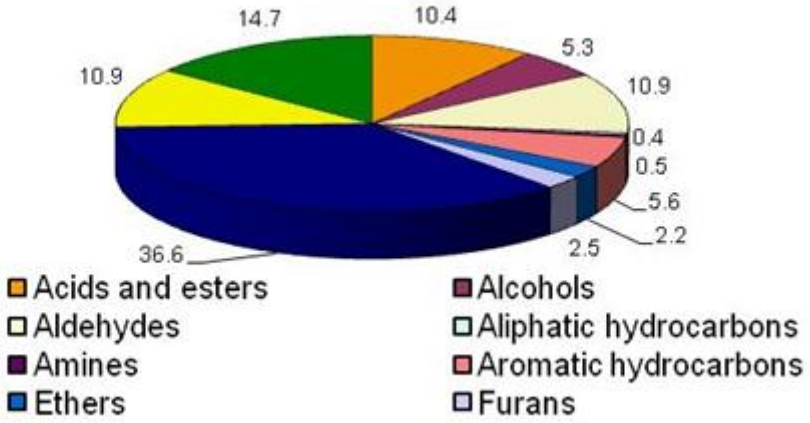

Figure 4. A representative chemical composition of bio-oil [31]

As a result of these oxygenated compounds, bio-oil has a low energy density and low miscibility with conventional petroleum fuels. Therefore, it cannot be used directly as a substitute for conventional petroleum fuels. Also, bio-oil cannot be distilled due to the significant formation of tar in the process [32]. Further, the presence of functional

groups decreases the stability of the oil, resulting in polymerization. A direct consequence is the increase of the viscosity of bio-oil with time, which raises concerns about the feasibility of using bio-oil as a substitute for petrochemical fuels. In addition to its instability, several other properties are considered to be problematic, including its low pH values, high water content, and ash [32, 33]. In contrast, petroleum crude is lean in oxygenated compounds and, therefore, most of the studies of its chemistry to date have been focused on adding functional groups to increase its activity. As a result, only limited knowledge exists for available techniques to remove functionality from highly-oxygenated compounds. Therefore, the removal of oxygen (deoxygenation) is considered to be the most intricate challenge we face today in converting bio-oil to a form that can be used more extensively as a fuel substitute.In this context, several processes have been investigated for upgrading bio-oil to produce hydrocarbon fuels and high-value chemicals.

The removal of oxygen (deoxygenation) and the addition of hydrogen (hydrogenation) to biomass-derived oxygenated compounds are essential for the transformation processes. Some of the key techniques for upgrading biomass-derived bio-oil can be summarized as follows.

Secondary pyrolysis

This is the simplest process with no catalyst involved for the deoxygenation of biomass oxygenates, but it has fairly low efficiencies. The concept behind this process is simply to route the pyrolysis vapor through a second reactor that is maintained at a high temperature. The thermal-cracking reaction initiated in the secondary reactor would

remove oxygen as H_2O, CO_2, and CO. Due to the thermodynamic nature of this reaction, increasing the residence time of the products in the reactor would result in the production of more thermodynamically-stable species, such as CO_2 and CO. The significant disadvantage of this method is the possibility of losing carbon as CO_2 and CO.

Catalytic upgrading

The catalytic upgrading process can be conducted in several different ways. The most common method is to obtain liquid bio-oil and inject it into a tubular reactor filled with catalyst to obtain a deoxygenated product stream. However, a reactor design with the direct feed of pyrolysis vapor into the catalyst became more popular due to the inefficacies of the tubular reactor due to the condensing and reheating processes. Different zeolites have been tested as catalysts in this process, and ZSM-5 has proven to be the most effective. ZSM-5 is a molecular sieve with 5.5 Å pore channels, which gives it unique selectivity for aromatic hydrocarbons.

The deoxygenation reaction on ZSM-5 is catalyzed by the acid sites of the catalyst. There are two types of acid sites, namely Bronsted and Lewis sites. Bronsted acid sites are said to be the catalytic sites of ZSM-5. Since the oxygenates that are produced in the pyrolysis reaction consist of aldehydes/ketones, alcohols, and carboxylic acids, the overall deoxygenation reaction can be subdivided into three key reaction categories, i.e., dehydration, decarbonylation, and decarboxylation. These reaction categories have important roles in selecting the right catalyst for upgrading the process. For the catalyst to be suitable for the deoxygenation process, it should catalyze all three

of the reactions that were mentioned. Even with the ZSM-5 catalyst, this process would not yield optimum results due to the hydrogen-deficient nature of the4 biomass (C:H < 1). To deal with this deficit, extraneous hydrogen must be supplied to the reactor, and this new process is called hydrodeoxygenation.

Hydrodeoxygenation

Hydroprocessing is a crucial step in the petroleum refining process, and it basically involves five types of reaction classes, i.e., hydrodenitrogenation (HDN), hydrodesulfurization (HDS), hydrodeoxygenation (HDO), hydrodemethylation (HDM), and hydrogenation (HYD) [34-36]. In a typical hydroprocessing process, the tendency of the hetero atom removal can be represented as HDS > HDO > HDN. Since there is no a significant amount of oxygen in petroleum crude, the chemistry of HDO has received little attention in the petrochemical industry [27]. However, since the most abundant heteroatom in bio-oil is oxygen, the HDO reaction will be dominant in a bio-oil hydroprocessing process. Many studies have been conducted on the HDO process, making it one of the most extensively-explored reactions related to the upgrading of bio-oil [34]. The HDO process has an undesired outcome, which is the hydrogenation of aromatic rings. Saturation of the aromatic rings is not economically favorable because it consumes large amounts of hydrogen and reduces the octane number of the fuel. Further, catalyst deactivation is a serious disadvantage of the HDO process. Generally, the products of hydrotreatment, such as water, ammonia, and hydrogen sulfide, are considered to be poisonous agents for the hydrotreating catalyst [37].

Most of the studies on HDO have been based on supported metal catalysts, such as Co-Mo, Ni-Mo, Ni-W, Ni, Co, and Pd loaded on alumina. Ideally, a suitable catalyst for HDO should perform two tasks, i.e., it should activate the hydrogen molecule and activate the oxygen group that is present in the compound. Activation of the oxygen group usually occurs on oxides of transition metals, such as Mo, W, Co, Mn, Zr, Ce, Y, Sr, and La, while the noble metals, such as Pt, Pd, and Rh, are known for their activation of hydrogen [38]. Most studies of HDO chemistry have been performed using model compounds, such as phenol, cresole, guaiacol, and napthol , which are abundantly present in bio-oil. Table (2) shows the HDO reaction pathways for phenol and cresole [39, 40]. According to above schemes, the prolonged hydrotreatment of oxygenates would yield more saturated cyclic hydrocarbons.

The overall objective and the central hypothesis

As described above, hydrodeoxygenation is an effective method for increasing the energy density and stability of bio-oil and for upgrading bio-oil to liquid hydrocarbons [21, 27, 34, 41-44]. However, the high oxygen content (35-40%) in biomass leads to an extremely high gaseous hydrogen requirement, which has a significant adverse effect on the economics of the process. Thus, thermal cracking is a more economically-attractive option. However, thermal cracking is inherently plagued by high yields of less-desirable, lower hydrocarbons and the formation coke, which result in the rapid deactivation of the catalyst [45-50].

Table 2. Proposed reaction pathways for HDO reactions of cresole and phenol

Oxygenate	Proposed hydrodeoxygenation reaction	Ref.
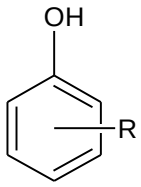 Cresole	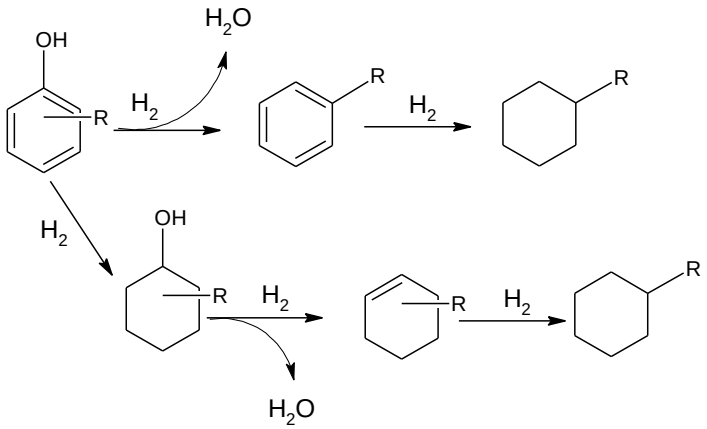	[39]
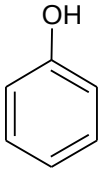 Phenol	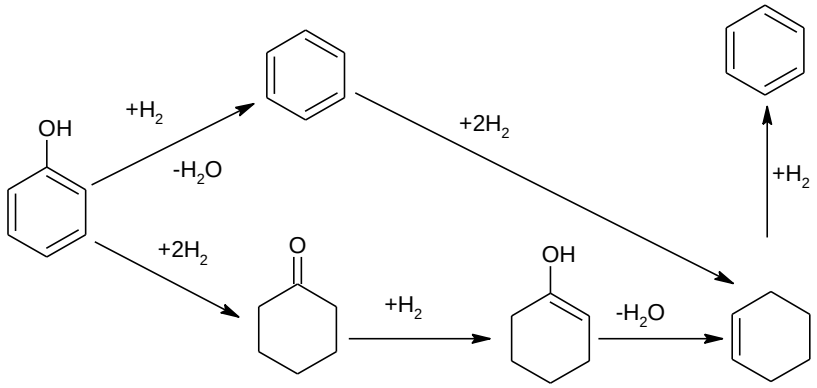	[51]
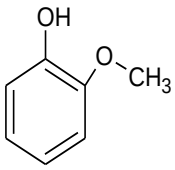 Guaicol	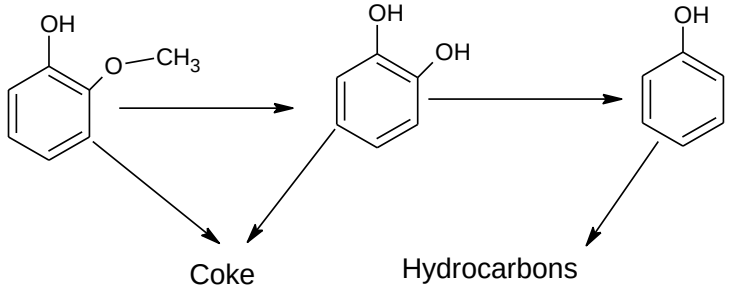	[37]

Low-severity hydrotreating or partial hydrodeoxygenation can be alternatives to full deoxygenation for improving the properties of bio-oils with low hydrogen consumption [52-55]. However, these options still require many of the features of full hydrotreating. Commercial H_2 production usually involves steam reforming technology, which uses natural gas as the feedstock [56-58]. Steam reforming is an energy intensive reaction, and the resulting H_2 is expensive. Therefore, the overall objective of this project was to discern whether it is possible to use methane as a substitute for H_2 in the deoxygenation of the oxygenates in biomass by gaining insights on the types and the extent of reactions that occur when biomasss oxygenates are pyrolyzed in the presence of methane and select catalysts.

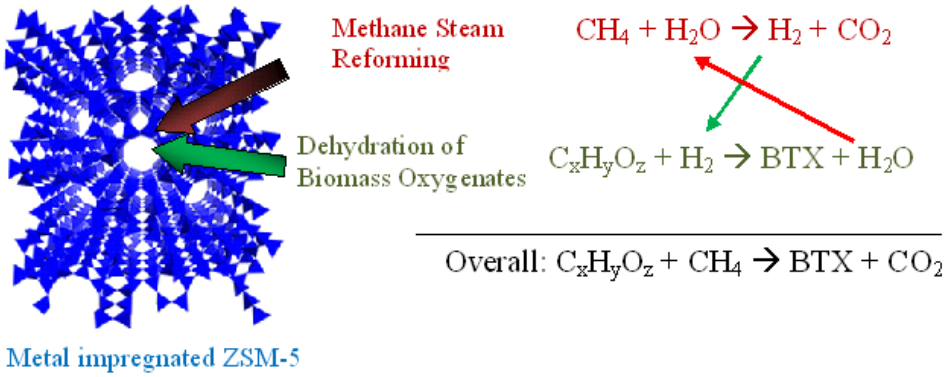

Figure 5. Proposed reaction scheme for methane coupled deoxygenation

The central hypothesis of the study can be summarized as follows: To avoid using expensive H_2 for upgrading bio-oil, lower alkanes, such as methane from natural gas and biogenic sources (and ethane and propane from petroleum refineries) can be

used as a cheaper source of H_2 in a direct coupling reaction with oxygenates to produce hydrocarbons. As shown in Figure 5, the crux of this concept is based on the premise that it is possible to couple two complementary reactions (methane steam reforming and aromatization with oxygenates dehydration) in a single reaction environment to harness the advantages of both reactions.

Reaction coupling is a basic concept that can be applied to balance the heat of reaction and shift the equilibrium of the reaction. Many of the studies relevant to reaction coupling can be found in literature. The oxidative steam reforming of hydrocarbons to produce H_2 involves a coupling of the strongly endothermic reaction of steam forming with the strongly exothermic oxidation reaction of methane combustion [59-61]. Oxidative conversion of ethane to ethylene couples endothermic cracking with exothermic oxidative conversion [62, 63]. The dehydrogenation of ethylbenzene in the presence of CO_2 couples the dehydrogenation reaction with the reverse water gas shift reaction, which is an energy-saving and environmentally-friendly process [64-66]. The equilibrium conversion of ethylbenzene to styrene can be improved greatly by the coupling of ethylbenzene dehydrogenation with nitrobenzene hydrogenation for simultaneous production of styrene and aniline [67].

The preceding overview of bio-oil upgrading and methane conversion clearly indicates that the production of hydrocarbon fuels or value-added chemicals from biomass is a hydrogen-consuming process, while the conversion of methane and lower alkanes is a hydrogen-producing process.

CHAPTER II

PROOF OF CONCEPT

Introduction

Industrial scale H_2 production is done via methane steam reforming. Steam reforming is an endothermic reaction that is generally catalyzed by $Ni/\gamma–Al_2O_3$, as shown in Equation (3).Deoxygenation of biomass is a hydrogen-deficient reaction for which a supplemental H_2 supply is required to sustain the production of hydrocarbons. Using glucose as a model biomass, this reaction can be represented as shown in Equation (4), which indicates that deoxygenation is an exothermic reaction.

$$CH_4 + 2H_2O \longrightarrow CO_2 + 4H_2 \quad (+)\ 164.99\ kJ \qquad (3)$$

$$C_6H_{12}O_6 + 57/16\ H_2 \longrightarrow 1/16\ C_6H_6 + 3/8\ C_7H_8 + 3/16C_8H_{10} + 3/16C_8H_{10} + 6H_2O \quad (-)146.83\ kJ \qquad (4)$$

$$C_6H_{12}O_6 + 57/64\ CH_4 \longrightarrow 1/16\ C_6H_6 + 3/8\ C_7H_8 + 3/16C_8H_{10} + 3/16C_8H_{10} + 135/32\ H_2O + 57/64\ CO_2 \quad (+)\ 0.11\ kJ \qquad (5)$$

If these two reactions were coupled together in such a way that Equation (3) provides necessary H_2 to the reaction in Equation (4), the resultant reaction can be represented as in Equation (5). According to the overall stoichiometry, the reaction is slightly exothermic. The low net heating value of Equation (5) suggests that the two reactions given in Equations (3) and (4) can be coupled to form an energetically efficient reaction in which the heat of the exothermic reaction provides the energy necessary for the endothermic reaction.

The overall goal of this study was to determine whether methane can be used as a hydrogen donor for the deoxygenation reaction so that a cheaper, viable alternative can be made available instead of using expensive H_2. When methane is introduced in an oxygenate-rich environment, several reactions that yield hydrocarbons can take place. It is hypothesized that, depending on the type of catalyst, the reaction schemes given in Equations (6), (7), and/or (8) could take place.

$$\left.\begin{array}{l} CH_4 \rightarrow BTX \\ C_xH_yO_z \rightarrow BTX \end{array}\right\} \quad (6)$$

$$\left.\begin{array}{l} CH_4 + H_2O \rightarrow H_2 + CO_2 \\ C_xH_yO_z + H_2 \rightarrow BTX + H_2O \end{array}\right\} \quad (7)$$

$$C_xH_yO_z + CH_4 \rightarrow BTX + H_2O + CO_2 \quad (8)$$

The scheme in Equation (6) represents two independent reactions in which methane and oxygenates are converted into hydrocarbons independently. Even though the direct conversion of methane occurs at high temperatures, it is quite possible for this reaction to proceed under mild conditions in the presence of specific transition metal catalysts [68]. The scheme given in Equation (7) represents the ideal reaction that is expected to occur (our central hypothesis). According to this scheme, methane steam reforming and biomass deoxygenation reactions take place simultaneously. Due to the cross coupling of products, such as H_2 and H_2O, the reactions are interdependent. Equation (8) represents the situation in which both methane and biomass oxygenates proceed through a carbon pool to form hydrocarbons.

Materials and methods

This study was conducted in a GC/MS system connected online with a micropyrolyzer. GC-MS analyses were performed using an Agilent GC 7890 coupled with an Agilent MS 5890 (Agilent Technologies, Santa Clara, CA, USA). The micro pyrolyzer used in this study was a CDS pyroporbe 5200 micro-reactor (CDS Analytical, Oxford, PA, USA).

The glucose that was used as the biomass substitute was in two isotopic forms. The C^{12} and C^{13} isotope-labeled glucose products were obtained from Cambridge Isotope Laboratories (Andover, MA, USA) and Sigma Aldridge, St. Louis, MO, USA, respectively). Both the CD_4 (deuterated methane) and the CH_4 used in the experiment were purchased from Cambridge Isotope Laboratories (Andover, MA, USA).

The insipient wetness technique was used to impregnate the catalyst with transition metals, i.e., Ni, Pt, Mo, and Ga. The amount of metal loaded were 5% w/w. Catalyst preparation was done according to the method given in Qui et al. [69]. Nickel nitrate hexahydrate , tetraammineplatinum (II) hydroxide hydrate, ammonium molybdate, and gallium nitrate were purchased from Sigma Aldridge, (St. Louis, MO, USA). The process variables identified for this experiment were substrate type, substrate amount, proton donor, proton donor concentration, pyrolysis temperature, catalyst temperature, pressure, catalyst type, catalyst weight, flow rate of products, trap purge time, and product yield. Proton donor and catalyst type were selected as independent variables, and product yield was selected as the dependent variable. The experiment was

repeated five times (n = 5) and one way ANOVA analysis was used to analyze data. All the inferences were made at α=0.05 significance level.

Testing of scheme given in Equation (6)

According to the literature, direct methane activation occurs prominently in the presence of Mo/ZSM-5 or Ga/ZSM-5 [70], and deoxygenation can occur even in the presence of ZSM-5 without any metal promoters [71]. In order to get a better idea about the effect of the transition metals on product yield, Ga/ZSM-5, Mo/ZSM-5, and Pt/ZSM-5 catalysts were tested in this study. In order to test this reaction scheme, glucose labeled with C^{13} was selected as the substrate, and C^{12} labeled CH_4 was used as the proton donor.

Testing of scheme given in Equation (7)

Many in-depth studies of the methane steam reforming reaction have been conducted. According to the literature, nickel catalyzes this reaction quite well [72]. Since pyrolysis media contain significant amounts of water, there is a great possibility for the scheme given in Equation (7) to take place. C^{13}-labeled glucose was used as the biomass substitute, and C^{12}-labeled methane was used as the proton donor. To understand the effects of transition metals, Ni/ZSM-5, Ga/ZSM-5, Mo/ZSM-5, and Pt/ZSM-5 were used as catalysts in this study. Carbon dioxide was used as the product of interest (response variable). Depending on the source, the mass spectrum corresponding to CO_2 may vary from 44 to 45 amu.

Testing of scheme given in Equation (8)

If the reaction given by Equation (8) takes place, it is best explained by the hydrocarbon pool mechanism in which the exchange of both carbon and protons occurs. In order to

confirm that protons from methane participated in the reaction, C^{12}-labeled glucose and CD_4 were used. In this study, benzene was used as the molecule of interest (response variable) to study both the proton and carbon transfers to its ring structure using mass spectral data. The relative abundances of mass fragments with 79, 80, 81, 82, and 83 amu were compared with the respective mass fragments of fully-deuterated benzene. Similarly, the study of carbon transfer was conducted with C^{13}-labeled glucose and C^{12}-labeled methane. The relative abundances of the mass fragments of benzene with 79, 80, 81, 82, and 83 amu were compared with the respective abundances of the mass fragments from ^{13}C benzene.

Results and discussion

When direct activation of C^{12} methane takes place, the molecular mass of benzene would be 78 g/mol, and, in the corresponding mass spectrum, amu 78 would appear as the most abundant. However, the direct deoxygenation of C^{13}-labeled glucose would produce benzene with a molecular mass of 84 g/mol, and its corresponding mass spectrum would indicate amu 84 as the most abundant mass fragment. If methane activation and glucose deoxygenation occur simultaneously, benzene with both molecular masses should be detected by the mass spectrometer. Figure 6 indicates that what was expected actually occurred when methane was introduced into the oxygenates. According to these results, the catalyst has a significant effect on the yield of C^{12} benzene, which is a product of direct methane activation. The catalyst without any metal (loading) did not activate C^{12} methane significantly. Despite the high variability of the relative abundances, 5% Ga, 5% Mo, or 5% Pt on ZSM-5 showed higher direct activation of methane.

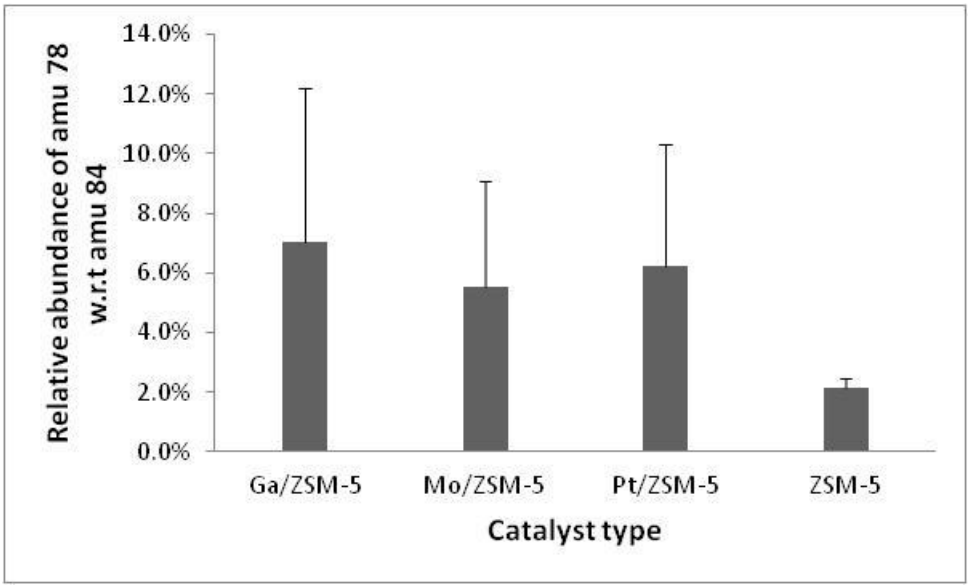

Figure 6. Relative abundances of 78 amu of C^{12} benzene at different catalyst (n=5, α=0.05)

Carbon dioxide is a product of both methane steam reforming as well as deoxygenation reactions. If CO_2 were produced as a result of steam reforming of ^{12}C methane, the abundant mass line in the mass spectrum of CO_2 would be 44 (i.e., the carbon in CO_2 originated from methane). When CO_2 was produced from the deoxygenation of ^{13}C labeled glucose (i.e., the carbon in CO_2 originated from glucose), the most abundant mass line in the mass spectrum would be 45 amu. As expected, the mass spectrum of the CO_2 that was produced when the methane was pyrolyzed with glucose contained both 44 and 45 mass lines, based on the type of catalyst that was used. The relative abundances of mass fragments 44 and 45 are shown in Figure 7, indicating the degrees to which these reactions occurred over the specific catalysts. The nickel-impregnated catalyst was expected to catalyze the methane steam reforming (coupled

oxygenates deoxygenation) reaction, and the results in Figure 7 prove that. The catalysts, i.e., Ga/ZSM-5 and Mo/ZSM-5, which catalyzed direct methane activation in the previous experiments did not show noticeable activity for steam reforming. Apart from nickel, Pt/ZSM-5 did show moderate activity for steam reforming. If deuterium from methane contributes to the hydrocarbon pool, it can be observed in the mass spectrum of benzene. The number of deuterium substitutions would increase the molecular mass of benzene, as shown in Table (3). According to the results shown in Figure 8, 'D' substitutions are quite prominent for Ga/ZSM-5 and Pt/ZSM-5.

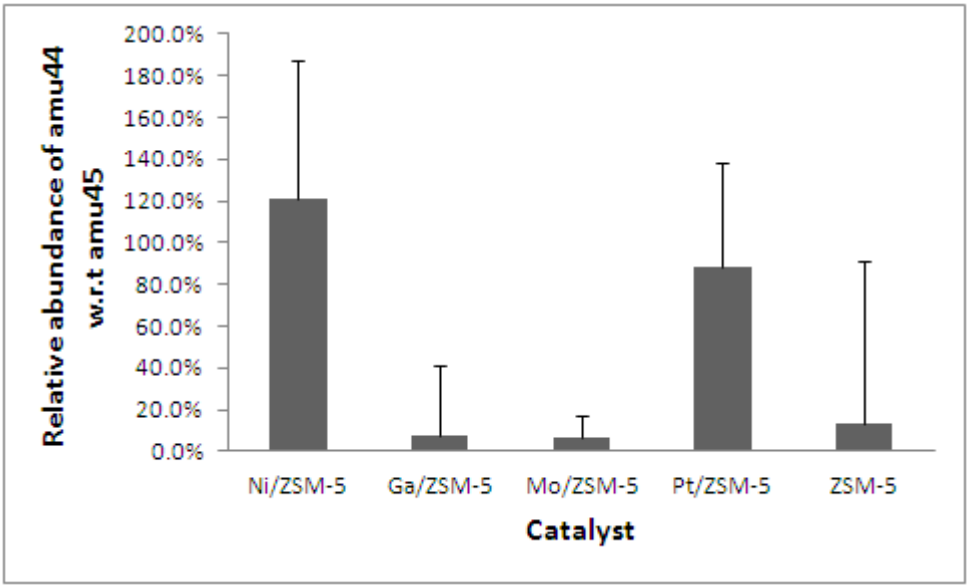

Figure 7. Yields of C^{12} labeled CO_2 and C^{13} labeled CO_2 (n=5, α=0.05)

Table 3. Mass values for different ring substitutions by deuterium and ^{12}C.

AMU	Deuterium substitution	^{12}C substitution
79	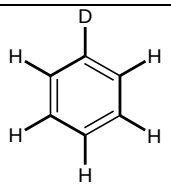	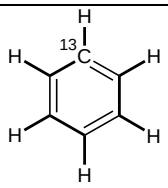
80	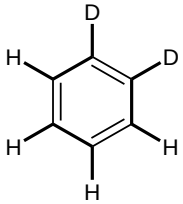	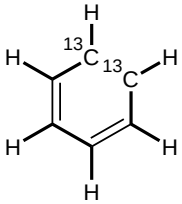
81	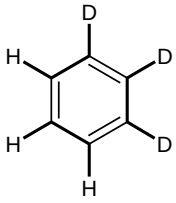	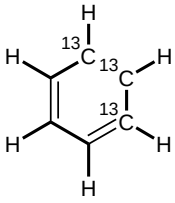
82	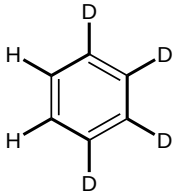	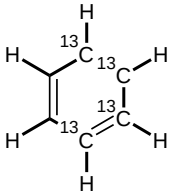
83	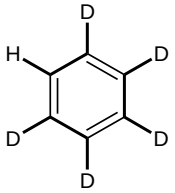	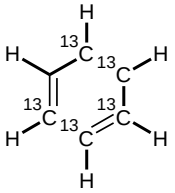
84	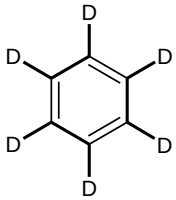	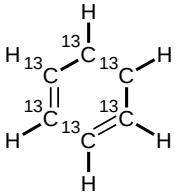

Also, it was noted that there was a direct correlation between 'D' substitutions and direct methane activation. The same catalyst that catalyzed direct methane conversion also catalysed the proton transfer reactions. This observation suggests that proton transfer is an integral part of the methane activation mechanism.

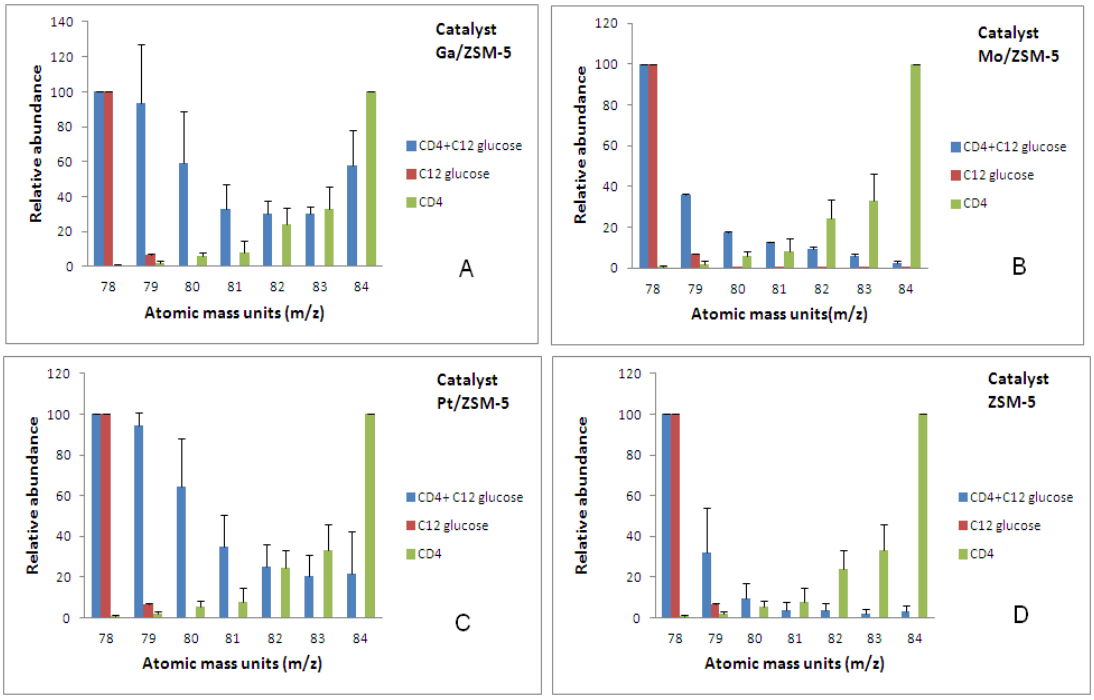

Figure 8. Deuterium substitution in the phenyl ring (n=5, p<0.05)

When the benzene ring was fully substituted by C^{13}, it had a molecular weight of 84 g/ mol, and, as a result, the most abundant mass fragment in the mass spectrum would be 84. If the C^{13} positions in benzene are substituted by C^{12} from methane, the mass would decrease. The decrease in the mass value with respect to each ^{12}C substitution is provided in Table (3). According to Figure 9, carbon substitution is not as prominent as 'D' substitution for most of the catalyst. There is a higher possibility of producing

benzene with amu 83 in the presence of Ga, Mo, and Pt catalysts. Conversely, the results of 'D' substitutions in Figure 9 do not indicate any substantial multiple substitutions of C^{12} in the benzene structure.

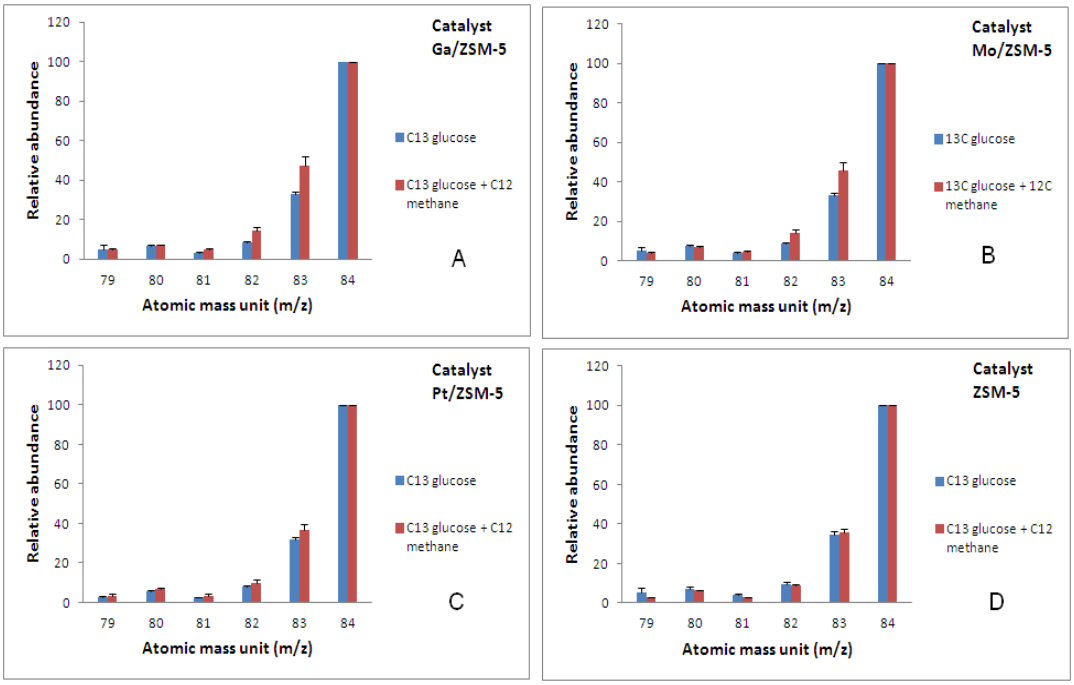

Figure 9. C^{13} substitution in the phenyl ring (n=5, α=0.05)

Specific conclusions

It can be concluded that, in the presence of Ga/ZSM-5 and Mo/ZSM-5, the reactions represented in Equation (6) take place. In the presence of Ni/ZSM-5, the cross coupling reaction given in Equation (7) was prominent, while it was marginal with Pt/ZSM-5. There is a good possibility that proton exchange occurred in the conversion process rather than carbon exchange. Proton exchange was prominent with the Ga/ZSM-5 catalyst.

CHAPTER III

THERMODYNAMIC MODELING OF GLUCOSE PYROLYSIS[*]

Introduction

A thermodynamic analysis is quite helpful in elucidating the equilibrium compositions of a pyrolysis reaction. At thermodynamic equilibrium, the concentration of each species in a chemical reaction reaches the theoretical maximum. Knowing the equilibrium composition is very important as a prelude to understanding the mechanics of the biomass pyrolysis process. This process is complex and, therefore, to better understand the underlying chemistry, biomass derivatives, such as glucose or its analogs are commonly used.

Glucose pyrolysis produces different types of oxygenated products, including furans, aldehydes, and carboxylic acids. With longer residence times, these products generally convert to significant amounts of aromatic hydrocarbons [73]. This conversion process can be represented in a scheme as shown by Figure 10. The primary products produced as a result of a short residence time are reported to be generated via two pathways, one of which is said to be the direct result of the dehydration of glucose and produces furan and its derivatives during the primary stage [74]. Various products that produced in the primary stage, such as aldehydes and ketones, are considered mainly to be the result of Grob fragmentation and retro aldol condensation reactions [75]. The

[*] Printed in part with permission from Gunawardena, D.A. and S.D. Fernando, *A Thermodynamic Equilibrium Analysis of Glucose Conversion to Hydrocarbons.* Chemical Engineering Communications, 2014. **201**(8): p. 1115-1124. Copyright 2014 Taylor & Francis.

pyrolysis of glucose is predominantly a free radical reaction, and it cannot be expected to reach equilibrium in short residence times. However, with longer residence times, such as those that have been observed in certain pyrolysis reactors, the reactions would reach thermodynamic equilibrium.

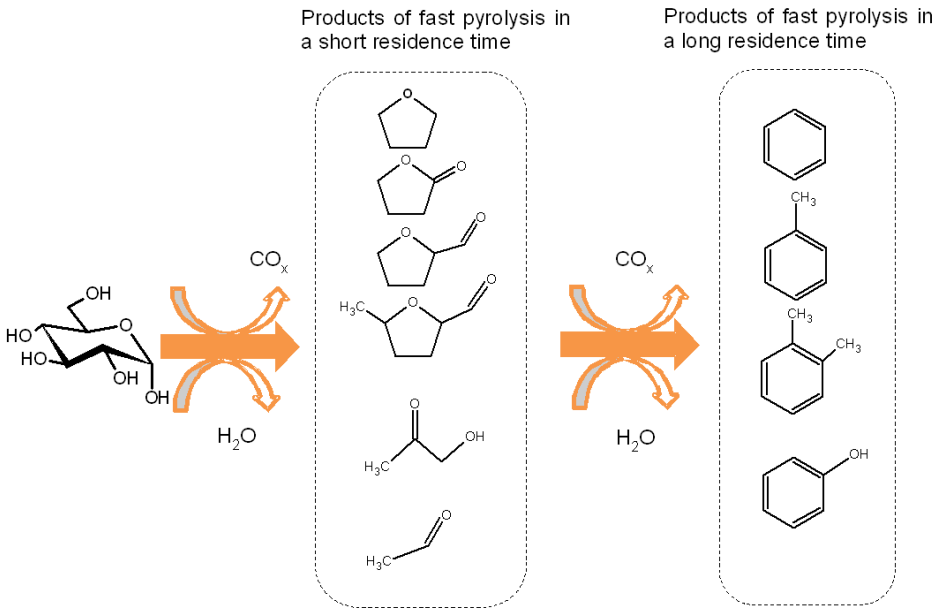

Figure 10. Reaction model for a pyrolysis reaction

For the pyrolysis process, a simple stoichiometric equation cannot be specified due to the complex nature of the process. However, when the stoichiometry of the reaction is not known, non-stoichiometric methods, such as free energy minimization, kinetic/dynamic modeling, and neural network methodology, can be used to determine the equilibrium composition. Since a pyrolysis system involves temperature and pressure as variables, it is more convenient to select the Gibbs free energy minimization technique, which traditionally has been solved by the Lagrange multiplier method. With

the development of powerful computational techniques, direct solutions can be obtained by successive quadratic programming (SQP) and generalized gradient (GRG) methods [76].

Materials and methods

To analyze the equilibrium composition of the pyrolysis gas mixture, a code written in Python (an open-source programming language) was used to run the Cantera software library. Cantera is an object-oriented software tool for solving chemical kinetics, thermodynamics, and transport processes problems, and it was developed by a team from the California Institute of Technology. Equilibrium composition was determined by Gibbs energy minimization using the Villars-Cruise-Smith algorithm [77]. Thermodynamic data of the species were calculated using a seven-coefficient polynomial developed by NASA, which is given in Equation (9) [78].

$$\frac{G_T^o}{RT} = a1(1 - \ln T) - \frac{a2}{2}T - \frac{a3}{6}T^2 - \frac{a4}{12}T^3 - \frac{a5}{20}T^4 + \frac{a6}{T} - a7 \quad (9)$$

All the values of the coefficients were obtained from Alexander Burcat's online database [78]. The thermodynamic data are valid for the temperature range of 200-6000 K. These coefficients were determined by using *ab-initio* density functional theory (DFT) on Gaussian software.

An experimental study was conducted in order to compare the theoretical results with experimental results. The experiment was conducted using a high-pressure, micro pyrolyzer (CDS pyroprobe 5200) connected in line with a GC/MS (Agilent 7890) system [79].The temperature of the reactor was maintained at 300-700 ^{0}C at 100 ^{0}C

intervals, and the pressure in the reactor was maintained at three gauge pressures, e.g., 0, 50, and 100 psi).

The theoretical model consisted of eleven species, such as C_6H_6, C_7H_8, C_8H_{10} (ethyl benzene), C_8H_{10} (xylenes), C_6H_5OH, CH_4, H_2O, C, CO_2, CO, and H_2. The mole fractions for all of the species were calculated considering that the mixture contained only these eleven species.

The total Gibbs energy, G_T, of the system can be expressed in terms of the standard Gibbs free energy and the fugacity of each individual component, as indicated in Equation (10) [80, 81]. Since fugacity also can be written as shown in Equation (11), the whole equation can be rearranged as shown in Equation (12). In this model, it was assumed that all of the components were in the gas phase and behave as ideal gases. Given these assumptions, we can treat the fugacity coefficient φ_i as unity.

$$G_T = \sum_{i=1}^{n} n_i \overline{G_i} = \sum_{i=1}^{n} n_i G_i^o + RT \sum_{i=1}^{n} n_i \ln\left(\frac{\hat{f}_i}{f_i^o}\right) \tag{10}$$

$$\hat{f}_i = \hat{\phi}_i * y_i * P \tag{11}$$

$$G_T = \sum_{i=1}^{n} n_i \Delta G_i^o + RT \sum_{i=1}^{n} n_i \ln(y_i) + RT \sum_{i=1}^{n} n_i \ln(P) + RT \sum_{i=1}^{n} n_i \ln\left(\hat{\phi}_i\right) \tag{12}$$

$$\sum_{i=1}^{n} n_i a_{ij} = b_j : j = 1 \ldots . K \tag{13}$$

In order to determine the minimum Gibbs free energy of the system, Equation (12) must be minimized. Since G_T (the objective function) is nonlinear, it was necessary to use a nonlinear optimization technique. The optimization problem was solved by

subjecting the objective function to a set of constraints. The set of non-linear constraints shown in Equation (13) can be obtained by considering the elemental mole balance of each compound in the equilibrium mixture. In this study C, H, and O were taken as elements of the equilibrium system, and their values were dictated by the C, H, and O compositions of glucose. The experiment was conducted as a full-factorial design with three replicates. The results were analyzed at $\alpha = 0.05$ significance level using Design-Expert software (Stat-Ease, Inc. Minneapolis, MN, USA).

Results and discussion

As described earlier, the system was treated as a mixture of 11 components, including C_6H_6, C_7H_8, C_8H_{10} (ethyl benzene), C_8H_{10} (xylenes), C_6H_5OH, CH_4, H_2O, C, CO_2, CO, and H_2.The system was allowed to reach equilibrium at different temperatures and pressures. At each pressure and temperature, the outcome of the optimization routine gives the number of moles for each compound. Since it is a gas-phase system, the partial pressure of each component is proportional to the mole fraction, and the results were analyzed in those terms.

Aromatic products

Figure 3 shows the equilibrium composition of the aromatic fraction, which consisted of C_6H_6, C_7H_8, C_8H_{10} (ethyl benzene), and C_8H_{10} (xylenes), at different temperatures and pressures. It is clear that the equilibrium aromatic mole fraction increased with increasing temperature. This trend further validated the fact that the formation of aromatics during the pyrolysis reaction was endothermic ($\Delta H > 0$). The pressure effect indicated that increasing pressure sharply increased the mole fraction of the aromatics.

According to the thermodynamic model, benzene is the most abundant product among all aromatic products considered.

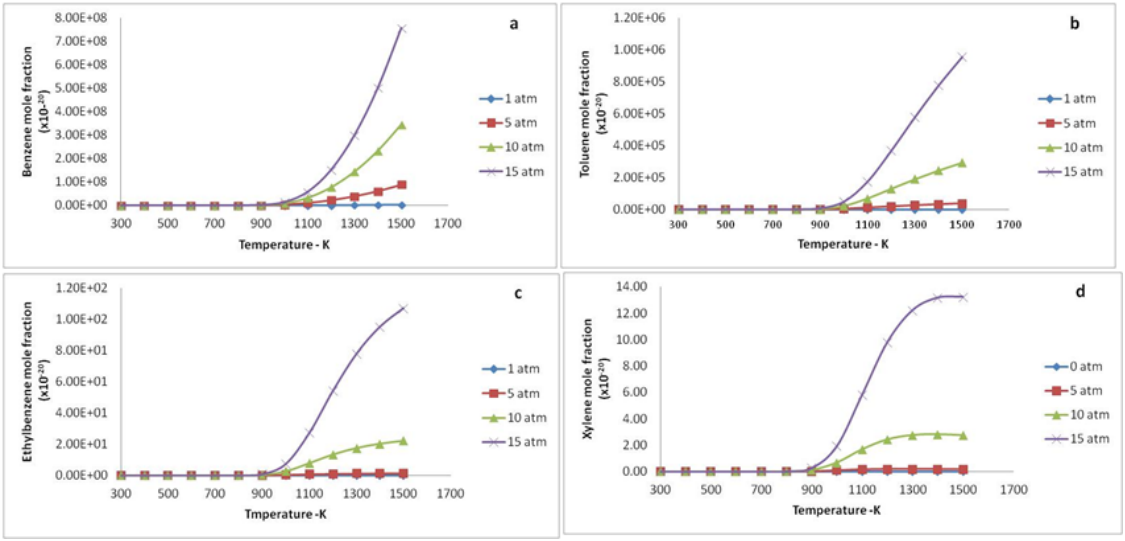

Figure 11. Aromatic mole fraction as predicted by the thermodynamic model: (a) benzene; (b) toluene; (c) ethylbenzene; (d) xylene; (e) phenol mole fractions

According to the experimental results shown in Figure 11, benzene is the highest mole fraction in the gas phase. The thermodynamically-predicted values were significanltly different from the experimentally-obtained mole fractions. This difference was an indication that the pyrolysis did not reach equilibrium in the experimental conditions. During this reaction the formation of aromatic products can be seen intermediates, which were reduced with time to more thermodynamically-stable species, such as CO_2, CO, H_2, and H_2O.

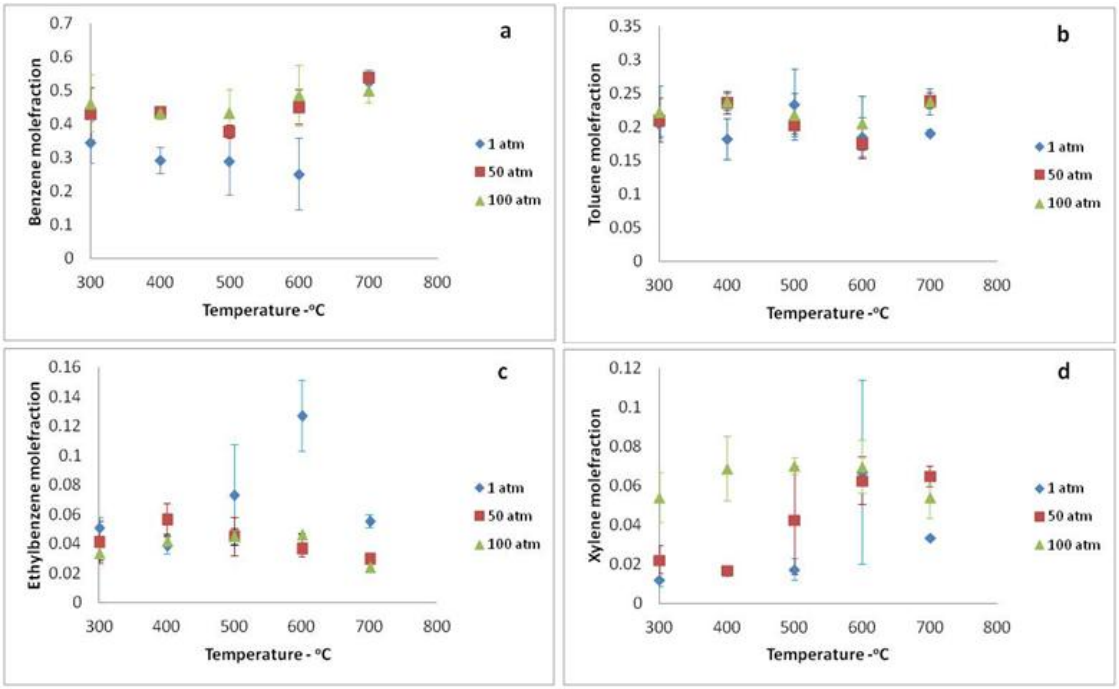

Figure 12. Experimentally-determined aromatic mole fraction: (a) benzene (b) toluene (c) ethylbenzene (d) xylene (n=3, α=0.05)

Close examination of the aromatic species in Figure 12 indicated that the temperature effect on mole fraction is not as significant as it was in the case of the theoretical results. According to Figure 12(a), the effect of pressure on the formation of benzene was significant.

Non-aromatic products

The non-aromatic products considered in the system were the most stable species. Therefore, at equilibrium, it can be expected that these species will be present in significant proportions. According to Figure 13(a), the equilibrium composition of methane reached a maximum in the range of 600 - 700 K and gradually decreased with increasing temperature. The effect of pressure was quite significant; an increase from 1

to 15 atm favored the formation of methane. The highest mole fraction reported for methane was 0.212 at15 atm and 700 K.

As shown in Figure 13(c) Carbon dioxide had a similar trend to methane, reaching its maximum mole fraction around 700 K after which it decreased as the temperature was increased. According to the analysis, the highest mole fraction of carbon dioxide was 0.242 at 15 atm and 800 K. The effect of pressure on the mole fraction of carbon dioxide also was significant, as was the case for methane, showing an increasing trend with increasing pressure.

Hydrogen can be removed from glucose in two ways, i.e., as hydrogen gas or as water. If hydrogen removal from the system takes place in these forms, the formation of hydrocarbon products will be limited significantly. As shown in Figure 13(b), the mole fraction of H_2 in the equilibrium mixture increased with temperature and reached its highest level of 0.49.

Carbon monoxide also follows a similar trend of increasing mole fraction as temperature was increased. Figure 13(d) shows that the equilibrium mole fraction of carbon monoxide was 0.50 at1500 K.

The behaviors of CH_4, CO_2, CO, and H_2 followed the equilibrium reaction given in Equation (6). It is clear from close examination of Figure 5 that increasing pressure increased the mole fraction of CO_2 and CH_4 and decreased the mole fractions of H_2 and CO. This agrees with Equation (14), which shows more moles on the right side than on the left side; hence, when the pressure is increased the reaction would tend to move to the left.

$$CH_4(g) + CO_2(g) \leftrightarrow 2CO(g) + 2H_2(g) \quad (14)$$

$$2CO(g) \leftrightarrow CO_2(g) + C(s) \quad (15)$$

$$CO(g) + 2H_2(g) \leftrightarrow H_2O(g) + C(s) \quad (16)$$

Water and carbon in the equilibrium model follow a similar trend according to Figures 13(e) and Figure 13(f). At 300 K, the equilibrium mole fraction of water was 0.853, but it decreased when the temperature was increased. The trend of carbon shows that the mole fraction at 300 K was 0.213. In a mixture made up of CO_2, CO, H_2, H_2O, and C, it can be expected that the two individual reactions given in Equations (15) and (16) are significant. Since the mole fractions of C(s) and CO_2 are decreased at higher temperatures, the equilibrium in Equation (15) should shift to increase the formation of CO. Similarly, in Equation (16) at high temperature, the equilibrium can be expected to shift to the left, making more CO and H_2 while the mole fractions of H_2O and C(s) would be decreased.

According to the experimental data shown in Figure 14, the mole fraction of CO was greater than those of all of the other non-aromatic products. The data show that increase in temperature decreased the mole fraction of CO and increased that of CO_2.

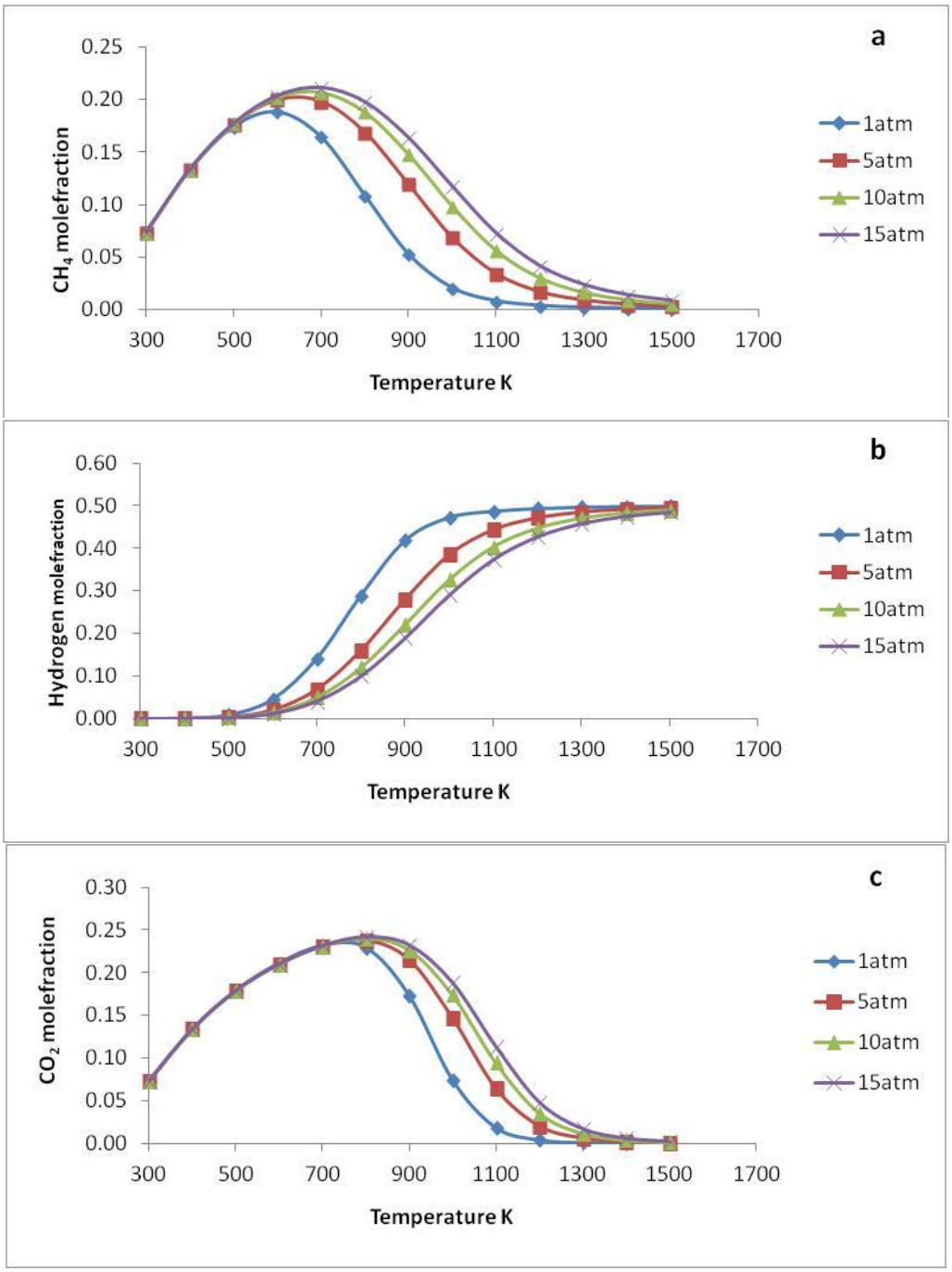

Figure 13. Non-aromatic mole fractions as predicted by the thermodynamic model: (a) methane (b) hydrogen (c) carbon dioxide; (d) carbon monoxide; (e) water (f) graphite mole fraction

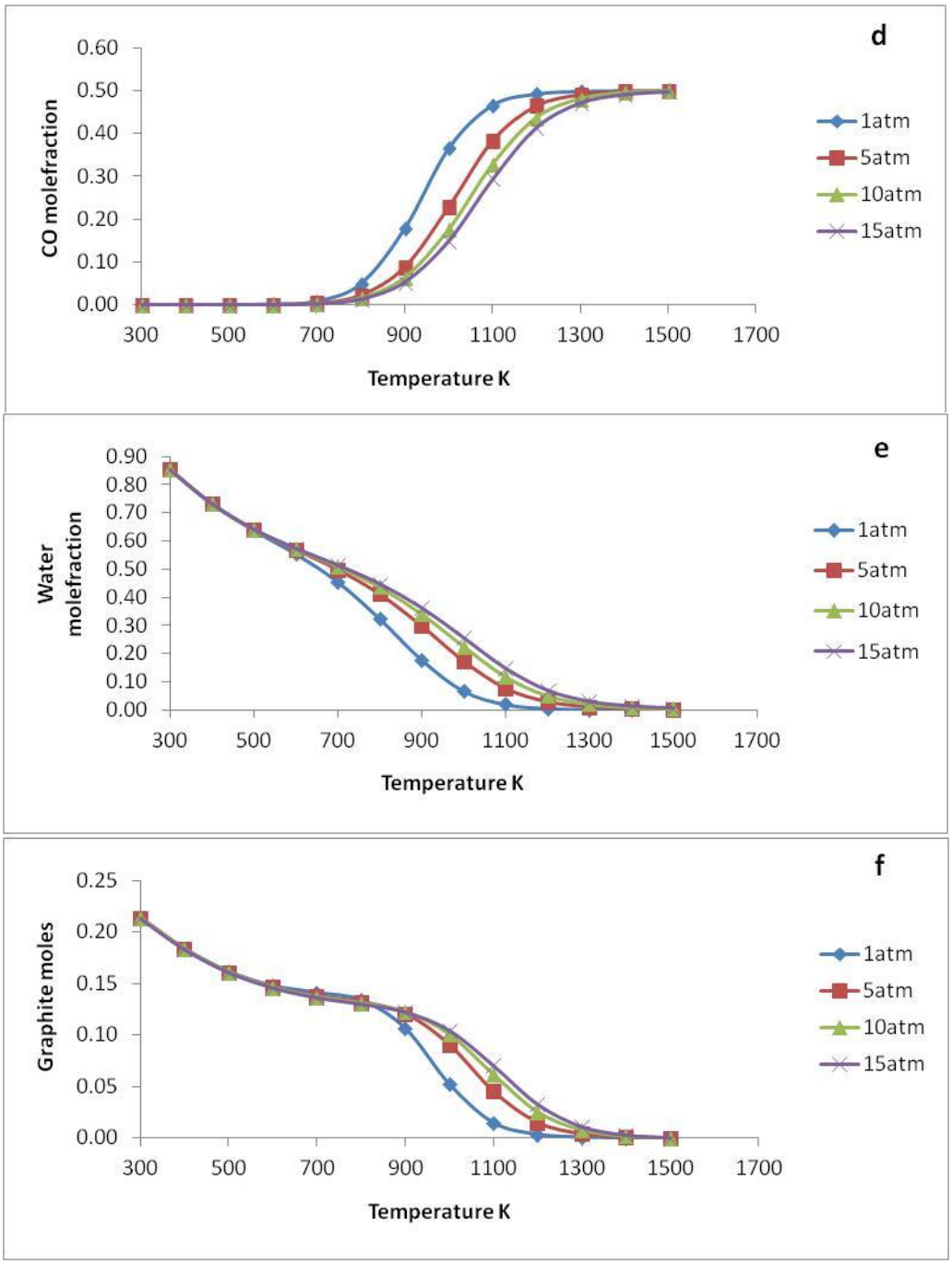

Figure 13. Continued.

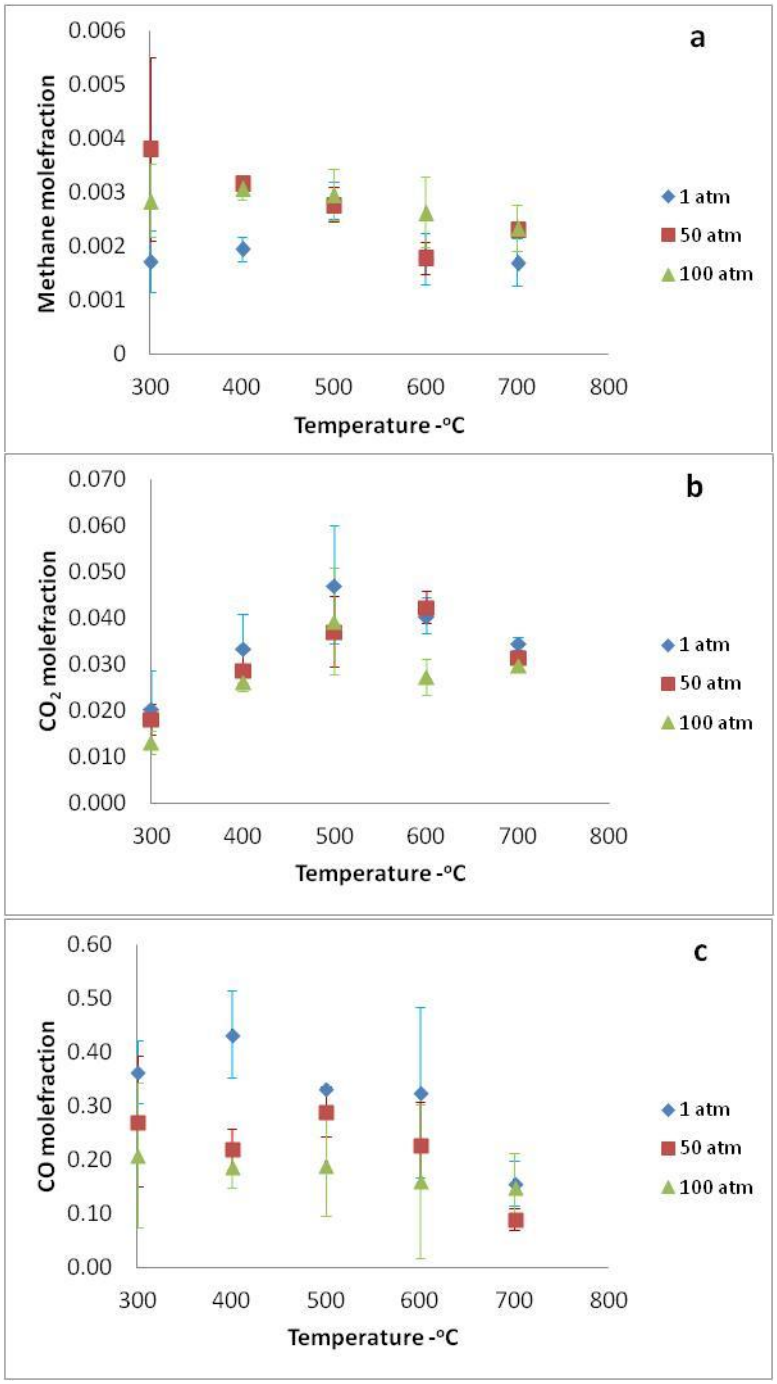

Figure 14. Experimentally-obtained non-aromatic mole fractions: (a) methane; (b) carbon dioxide; (c) carbon monoxide (n=3, α=0.05)

Specific conclusions

A system with 11 species was considered in this thermodynamic equilibrium model. The analyses indicated that an aromatic fraction was not present in significant quantities in the equilibrium mixture. According to the observations, the system at thermal equilibrium had a great tendency to move toward thermodynamically-stable species, such as CH_4, CO_2, H_2O, CO, H_2, and C. At low temperature, the equilibrium mixture was dominated by the H_2O, C, CH_4, and CO_2 species. Increasing the pressure on these products resulted in increasing their mole fractions. At high temperatures, the system favors the production of H_2 and CO, and increasing the pressure was not favorable for producing these species.

CHAPTER IV

CATALYST SCREENING STUDY

Introduction

Transition metals are known to have good catalytic properties for various chemical reactions, such as deoxygenation, dehydration, and methane activation. Since various metals and metal oxides can act as catalysts, a screening study would yield information that would be helpful in identifying the best catalyst for the methane coupled deoxygenation process. Since this study involved the coupling of two reactions, it was important for the catalyst to have a balance of two functionalities, i.e., deoxygenation and activation of methane by heterolytic cleavage of C-H bonds. The Bronsted acid sites of ZSM-5 catalyze the deoxygenation reaction [82], while transition metals, such as Mo and Pt, impregnated on a support such as alumina or ZSM-5 catalyze methane activation.

The refractory nature of methane makes it very difficult to use in a chemical reaction under mild conditions. Methane activation warrants rigorous reaction conditions, such as higher temperatures or oxidative environments [83]. Due to its strong C-H bond dissociation energy (104 kcal/mol), the thermal activation of methane occurs at temperatures above 1030 ^{o}C [84]. The direct conversion of methane to alkanes, aliphatics, or aromatics is thermodynamically highly unfavorable. The Gibbs free energy values given in Table (4) indicate that these reactions are not naturally spontaneous. Therefore, to circumvent these issues, the reaction either must be forced by providing the

required energy or the reaction path must be altered in such a way as to avoid the thermodynamic barrier [85]. It has been found that adding species, such as H_2O, CO_2, or O_2, on the reactant side with methane makes the conversion of methane thermodynamically favorable. It also has been found that methane can be converted to hydrocarbons in the presence of metals, such as Mo, Pt, and Ga on ZSM-5 [86]. Since the methane dehydro-aromatization reaction is not thermodynamically favorable below a temperature of1313 K, the production of aromatics using different transition metals at lower temperatures must result from a different thermodynamic pathway. In-depth studies using Mo have indicated that MoO_3 actually participates in the reaction as a reactant rather than a catalyst.

Table 4. Gibbs free energy of the reactions at different temperatures: The data were obtained from Yaws thermal database [87]

Reaction	400 K	600 K	800 K	1000 K
$2CH_4 \leftrightarrow C_2H_6 + H_2$	70.21	71.55	72.02	71.88
$2CH_4 \leftrightarrow C_2H_4 + 2H_2$	158.12	133.66	107.48	80.50
$6CH_4 \leftrightarrow C_6H_6 + 9H_2$	397.65	319.36	233.34	143.56

$CH_4 + H_2O \leftrightarrow CO + H_2$ ($\Delta_rG_{T=1000K}$ = -27.13 kJ/mol) (17)

$CH_4 + CO_2 \leftrightarrow 2CO + 2H_2$ ($\Delta_rG_{T=1000K}$ = -24.51k J/mol) (18)

$CH_4 + 1/2O_2 \leftrightarrow CO + 2H_2$ ($\Delta_rG_{T=1000K}$ = -219.96 kJ/mol) (19)

When deoxygenation occurs in the presence of methane, it can be expected that methane conversion reactions, as given in Equations (17) and (18) also taking place. Since dehydration is one of the prominent reactions that take place in deoxygenation, a

significant amount of H_2O is present in the reaction medium. Therefore, in the presence of a suitable catalyst, it can be expected that steam reforming also occurs. The goal of this study was to determine the best catalyst to couple Equation (17) with Equation (20) to create a cross-coupling reaction in which the necessary H_2 for deoxygenation is provided by the steam reforming reaction, while the necessary H_2O for the steam reforming reaction is provided via the deoxygenation reaction.

$$C_xH_yO_z + H_2 \longrightarrow C_aH_b + H_2O \quad (20)$$

Materials and methods

Generally, the pyrolysis of biomass, cellulose, or glucose produces a complex mixture of oxygenates, and it is quite difficult to maintain a consistent composition for long periods of time. For a quantitative study, it is important to maintain a consistent stream of oxygenates into the reactor. Furan is a major product of the pyrolysis of any cellulosic biomass. Therefore, for the purpose of modeling the deoxygenation reaction, furan was used as the model oxygenate in this experiment.

Furan (Sigma Aldridge) was injected into a preheated chamber by using a syringe pump (New Era Syringe pumps, NY). The volatilized furan was mixed with either helium or with a stream of helium and methane, as shown in Figure 15. The flow rate of the gas was maintained at 35 ml/min. Methane was diluted with helium at 10%V/V. The weight hourly space velocity (WHSV) of furan was 3.37 h^{-1}. The catalytic reactor was a quartz tube that was 10 cm long and had an OD of 6 mm. Twenty-five milligrams of catalyst were used in each run.

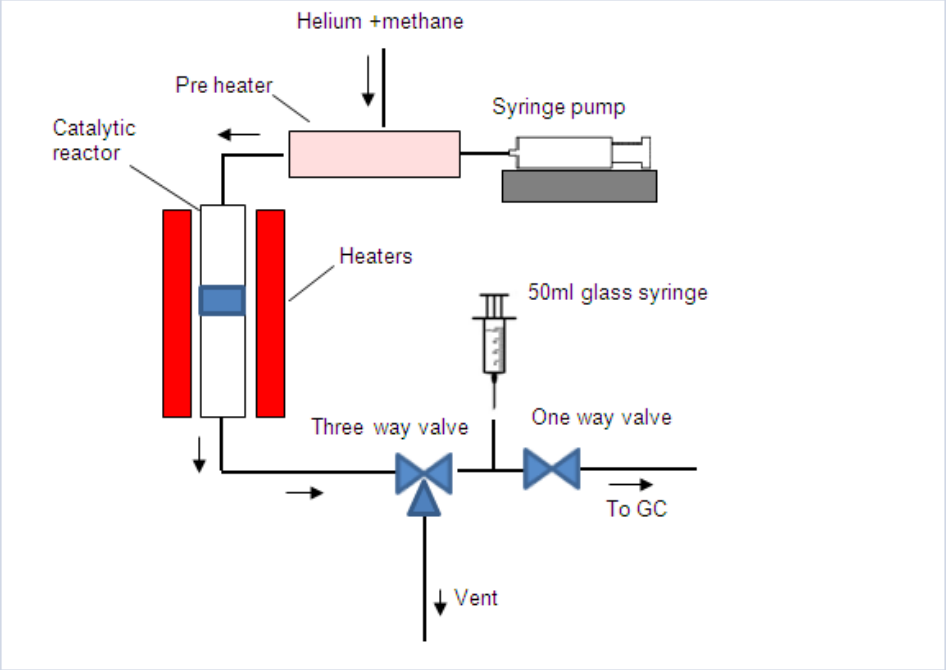

Figure 15. Schematic diagram of the reactor system used in the study

The ZSM-5 catalyst (SiO_2/Al_2O_3 = 30, Zeolyst Corp.) was used as a support, and it was received in the NH_4ZSM-5 form. The catalyst was calcined at 500 ^oC for 4 hr to transform it to HZSM-5. The M-HZSM-5 (M = Mo, Ga, Pt, Ni, Cr) was prepared by impregnating the metal salts to achieve different loading levels, i.e., 5%, 2%, and 1%. An aqueous solution of each metal was prepared by dissolving ammonium molybdate, gallium III nitrate, ammonium tetracholoroplatinate, nickel III nitrate hexahydrate, and chromium III nitrate. After impregnating with the salt solution, the support was dried at 50 ^oC for 4 hr and calcined at 500 ^oC for another 4 hr. The platinum and nickel catalysts were reduced in a H_2 stream (50 ml/min) for 2hr at 500 ^oC before being used.

The GC-MS analysis was performed using an Agilent 7890 GC equipped with the mass detector 5890 (Agilent Technologies, Santa Clara, CA, USA). The column

used for the GC/MS analysis was CP-Sil PONA CB (100 m, 0.25-mm OD, 0.5-μm ID). Gas samples were introduced via a 50-ml glass syringe. The GC was equipped with a gas sampling valve to inject the sample to the GC. Gas samples were collected 5 min after the reaction began. Coke deposition on the catalyst was quantified via the thermogravimetric analyzer (TGA Q50) (TA Instruments).

Furan conversion was calculated according to Equation (21), where N_o is the total number of furan moles fed into the reactor, and N_f is the unreached furan moles, which were quantified from the chromatogram. The selectivities of the catalytic reaction for benzene, toluene, ethylbenzene, and xylene (BTEX) were calculated considering the carbon balance. Selectivity was calculated according to Equation (22) given below, where N_i is the number of moles of the i^{th} product, and 'n_i' is the number of carbon atoms in the respective compound.

$$\text{Furan conversion } (X_{furan}) = (N_o - N_f)/N_o \quad (21)$$

$$\text{Selectivity of products} = n_i.N_i/(\Sigma n_i.N_i) \quad (22)$$

The experiment was conducted as a full-factorial design with three replicates. The results were analyzed at $\alpha = 0.05$ significance level using Design-Expert software (Stat-Ease, Inc. Minneapolis, MN, USA).

Results and discussion

The hydrodeoxygenation of furan to aromatics given in Equation (23) is highly exothermic (ΔH^o_r = -455.6 kJ/mol), while the methane steam reforming reaction shown in Equation (17) is moderately endothermic (ΔH^o_r = 205.8 kJ/mol). By coupling the two

reactions, the overall reaction given in Equation (24) was still substantially exothermic (ΔH^{o}_{r} = -249.8 kJ/mol). The thermodynamic properties of these reactions elucidate the behavior of the overall reaction at different temperatures. Figure 16 shows that the Gibbs free energy of the steam reforming reaction was positive for temperatures less than 890 K, indicating highly unfavorable conditions for its occurrence. However, to circumvent the free energy barrier, the reaction can be maintained at temperatures greater than 890 K despite that the fact that heat of reaction indicates that it is an exothermic reaction.

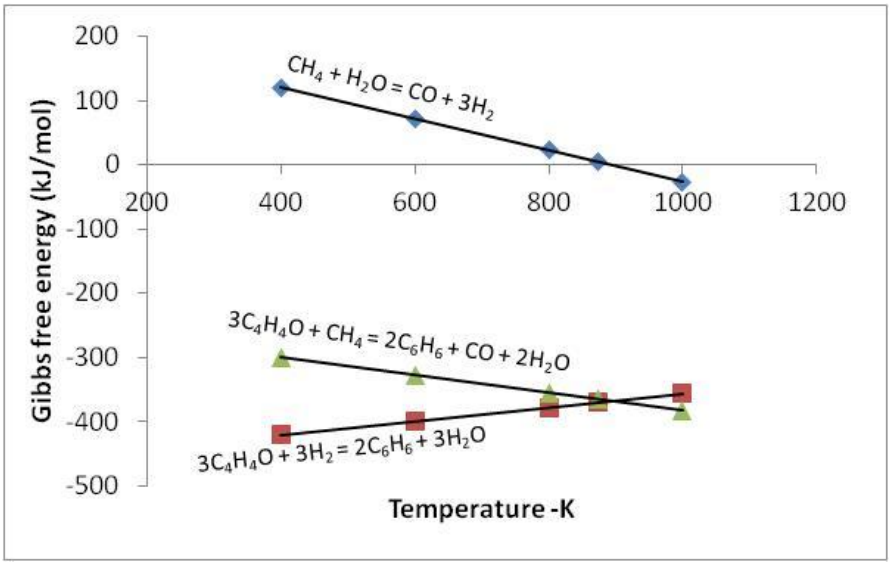

Figure 16. Gibbs free energies of the reactions at different temperatures

$$3C_4H_4O + 3H_2 \leftrightarrow 2C_6H_6 + 3H_2O \quad (23)$$

$$3C_4H_4O + CH_4 \leftrightarrow 2C_6H_6 + CO + 2H_2O \quad (24)$$

Furan is said to be thermally stable for a wide range of temperatures, and, in our experiment, no furan conversion was observed without the presence of a catalyst.

Several studies have been conducted to assess the conversion of furan to hydrocarbons using the HZSM-5 catalyst. According to Huber et al., furan undergoes two reaction paths on an acid catalyst such as HZSM-5, i.e., Diels-Alder condensation and decarbonylation [88]. As a result of Diels-Alder condensation, furan would be converted to benzofuran and water [82]. Subsequently, benzofuran would undergo further decarbonylation to produce benzene and other products with large molecular weights. These heavy products are responsible for the formation of coke on the catalyst. In the decarbonylation route, furan is converted to an allene as the primary product, and it would subsequently be converted to benzene [89]. In the comparison of these two paths, it can be pointed out that decarbonylation would be a better route for hydrocarbon formation because the Diels-Alder condensation would result in the formation of more coke. The decarbonylation of furan, as shown in Equation (25), is thermodynamically favorable over a wide range of temperatures. Therefore, in the presence of an acid catalyst, decarbonylation can be considered as the predominant reaction.

$$2C_4H_4O \leftrightarrow C_6H_6 + 2CO + 2H_2 \qquad (\Delta_r G_{T=1000K} = -338.5 \text{ kJ/mol}) \qquad (25)$$

The selection of the catalyst for this study basically involved two categories, i.e., 1) oxides, such as Ga_2O_3, MoO_3, and Cr_2O_3, which are known to activate methane by going through heterolytic C-H bond splitting [90, 91]and 2) metals, such as Pt and Ni, which are known to catalyze the steam reforming reaction [92]. While the direct activation of methane can make a positive contribution to the total hydrocarbon yield, our goal here was to exploit the synergistic effects of methane activation and furan decarbonylation to augment the hydrocarbon yield.

Since ZSM-5 provides an acidic medium, methane activation would produce CH_3^+ and H^- as a result of heterolytic C-H bond cleavage. Therefore, it can be expected that carbenium ions would initiate an electrophilic attack on furan, which has a lone pair of electrons on its oxygen. By incorporating a steam reforming catalyst, we expected to couple the methane steam reforming reaction with the furan deoxygenation reaction to generate a cross-feeding reaction to increase the production of hydrocarbons.

Ga_2O_3-impregnated catalyst

Gallium promoted ZSM-5 has been reported extensively as a bi-functional catalyst. It has been studied in processes, such as direct methane aromatization [93], decarboxylation [94], and dehydration reactions [95]. From the numerous studies of methane aromatization that have been conducted over the Ga/ZSM-5 catalyst, it is clear that Ga_2O_3 is responsible for catalyzing dehydrogenation and that the acid sites are responsible for oligomerization [94]. Recently, gallium-promoted ZSM-5 has been used to upgrade bio-oils and pyrolysis vapor. These studies have concluded that Ga on ZSM-5 catalyzes olefin oligomerization and decarbonylation [94, 96].

The results of our study, given in Figure 17, indicated that the conversion of furan decreased as the Ga loading increased, irrespective of whether the reaction included methane or was methane free. This trend of decreasing conversion with increasing Ga loading can be caused by the reduction of the surface area of the HZSM-5 catalyst as a result of higher loading. However, the acidity data in Table (5) show a clear trend of increasing Bronsted acidity with increasing Ga loading. A similar observation was made by Gao et al. , who has reported an Temeprature Programmed Desorption

study using ammonia on Ga/ZSM-5 [96]. Therefore, it can be deduced that increasing acidity has a negative effect on furan conversion. Figure 17 also shows that there was a significant decrease in furan conversion when methane was coupled as opposed to methane-free conditions. This interesting behavior could have been caused by the competition between methane and furan for surface adsorption.

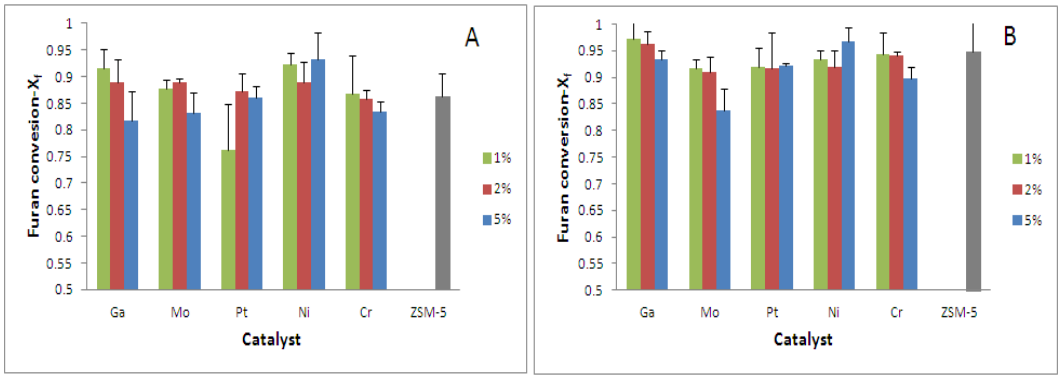

Figure 17. Furan conversion with different metal catalysts with different loading values: (A) methane environment; (B) methane-free environment (n=3, α=0.05)

It was pointed out earlier that Ga_2O_3, one of the known catalysts for direct methane aromatization, can produce more aromatic products. The selectivity data in Figure 18 show that having methane in the medium significantly increased the selectivity toward BTEX. The highest BTEX selectivity for the Ga catalyst was 5.93% for 5% gallium loading. This behavior of increasing BTEX selectivity while decreasing furan conversion with respect to increasing Ga loading in the presence of methane indicated that direct methane aromatization is an independent reaction that occurs concurrently with furan conversion.

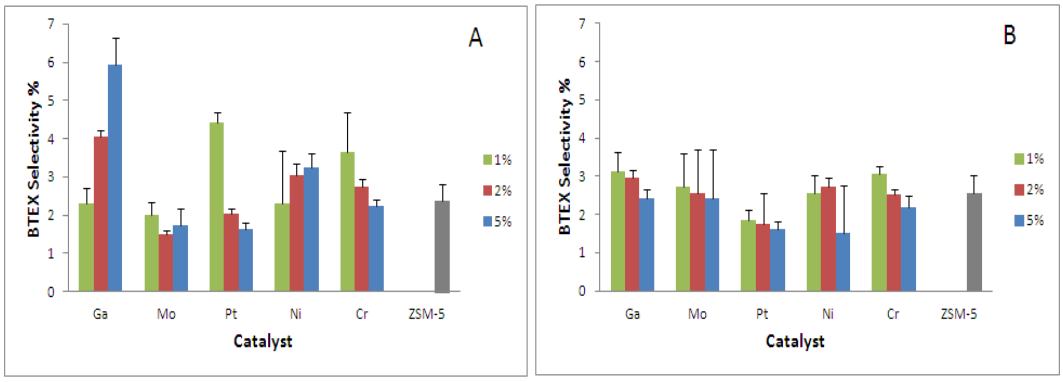

Figure 18. Selectivity toward BTEX using different catalysts: (A) with methane (B) without methane (n=3, α=0.05)

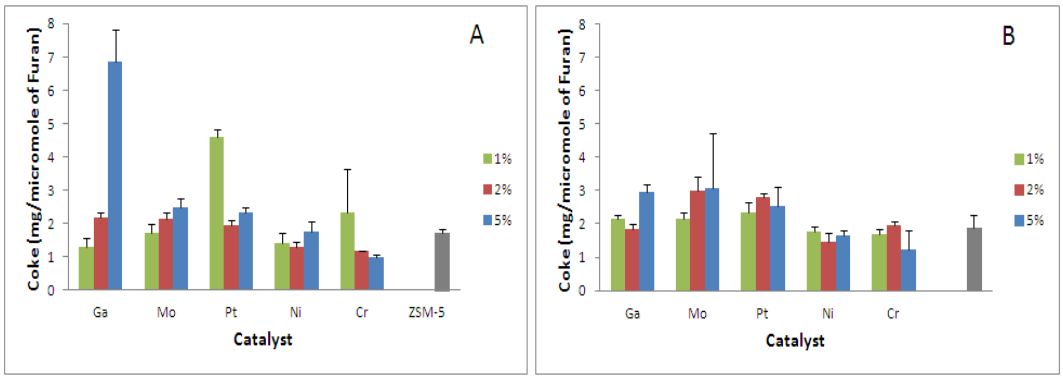

Figure 19. Coke deposition on different catalysts: (A) with methane (B) without methane (n=3, α=0.05)

The increased selectivity toward BTEX with the increase in acidity further justified the observed trend, i.e., methane aromatization occurred via direct methane coupling. The carbon formation on the surface of the catalyst also followed a similar trend to that of BTEX selectivity. Figure 19 shows that, in the methane environment, the highest carbon formation was reported for a gallium loading of 5%.

Table 5. Bronsted acidity of pure ZSM-5 catalyst and ZSM-5 catalyst impregnated with Ga_2O_3

Property	ZSM-5	1% Ga/ZSM-5	2% Ga/ZSM-5	5% Ga/ZSM-5
Bronsted acidity (mmol/g)	124.4	95.7	112.5	130.8

MoO_3-impregnated catalyst

Molybdenum-impregnated catalysts were prepared using ammonium molybdate. Calcination at 500 ^oC led to the formation the MoO_3 phase on the ZSM-5 catalyst. Although there is no consensus on the location of the Mo species on the catalyst, it has been reported that the factors that influence the location are the concentration of the Mo and the calcination temperature [90]. Previous studies conducted on Mo-promoted zeolite catalysts have indicated that Mo disperses into channels when the loading is less than 5%. Further, these studies concluded that Mo loadings greater than 5% would disperse Mo on the external surface. These observations led us to expect increased pore interruptions as the Mo loading increased. Studies in which methane was used with an MoO_3 catalyst indicated that the methane aromatization reaction proceeded through an induction period in which MoO_3 undergoes reduction to form MoO_2, subsequently being converted to the more stable form of Mo_2C.

It is believed that Mo_2C catalyzes direct methane aromatization. When molybdenum is used, Mo^{6+} would act as the hydride acceptor to form $[Mo\text{-}H]^{5+}$ and CH^{3+} [97]. Figure 17 shows that Mo had the same behavior that was observed for Ga. For instance, when the Mo loading was increased, furan conversion decreased in both

the methane environment and the methane-free environment. Based on a comparison of the acidity data given in Table (6), it can be inferred that increasing acidity is not favorable for furan conversion with Mo/ZSM-5. Also, it can be seen very clearly that there was a significant decrease in furan conversion when methane was introduced.

Table 6. Bronsted acidities of pure ZSM-5 catalyst and ZSM-5 catalyst impregnated with MoO_3

Property	ZSM-5	1% Mo/ZSM-5	2% Mo/ZSM-5	5% Mo/ZSM-5
Bronsted acidity (mmol/g)	124.4	111.3	148.7	181.1

The argument that was used for gallium also can be used here, since, in the methane environment, two reactions compete for surface adsorption, i.e., the methane aromatization reaction and the furan conversion reaction. The selectivity data for Mo/ZSM-5 given in Figure 18 show that selectivity for BTEX decreased as the Mo loading increased in the methane-free environment. However, when methane was introduced, the selectivity was less than it was for the methane-free condition. Therefore, it was concluded that direct methane aromatization was not a prominent reaction when Mo was used. It also was observed that coke formation (on the Mo/ZSM-5 catalyst) increased as the Mo loading increased. There was no significant increase in coke formation when methane was introduced.

Cr_2O_3-impregnated catalyst

Chromium can exist in multiple oxidation states, i.e., (II), (III), (V), and (VI). According to the procedure that was followed, it is expected to be in the (III) state [105]. According to some earlier studies, the most stable oxidation states of Cr are (III) and (VI) for which monochromate would be the most abundant under low loading conditions. Chromium has been reported extensively as a catalyst for the dehydrogenation of alkanes in oxidative and non-oxidative environments [98]. Cr also has been reported as a polymerization catalyst and a photocatalyst.

As was observed for Ga_2O_3 and MoO_3, the acidity values of Cr_2O_3 (Table 7) increased as the oxide loadings increased. The increase in acidity implies that there was an increase in surface hydroxyl groups, which contribute to Bronsted acidity. Methane activation by Cr/ZSM-5 is less than it is for Mo/ZSM-5 [99]. Figure 17 shows that the conversion of furan decreased from 94.3% at 1% Cr to 89.8% at 5% Cr in the absence of methane. The same trend was observed when methane was present. While catalyst pore interruptions can be considered to have a significant effect, furan conversion is affected greatly by the acidity of the catalyst. Figure 18 shows that the selectivity for BTEX decreased as Cr loading increased and that the change in selectivity when methane was coupled was marginal. The formation of coke on Cr_2O_3 can be considered to be low compared to many catalysts, and the lowest coke loading reported in the presence of methane was for 5% Cr.

Table 7. Bronsted acidity of pure ZSM-5 catalyst and Cr_2O_3-impregnated ZSM-5 catalyst

Property	ZSM-5	1% Cr/ZSM-5	2% Cr/ZSM-5	5% Cr/ZSM-5
Bronsted acidity (mmol/g)	124.4	55.6	192.5	228.8

Pt-impregnated catalyst

Platinum is not easily oxidized, and it exists as metal clusters on the surface of the ZSM-5 catalyst support. As a transition metal, Pt can catalyze many reactions, including the direct methane aromatization reaction [91], the methane steam reforming reaction [100], and the water gas shift (WGS) reaction [101]. Since Pt is not considered to be a favorable catalyst for direct methane aromatization, we can rule out the effect of Pt on BTEX formation (via direct methane coupling). However, Pt does have some catalytic properties in the steam reforming reaction. Figure 17(A) shows that the effect of Pt loading on the decarbonylation reaction can be considered to be insignificant since the furan conversion was constant. However, Pt loading had a significant impact on furan conversion when methane was introduced into the system. Unlike the Ga-, Mo-, and Cr-loaded catalysts, Pt/ZSM-5 showed an increasing trend in furan conversion with metal loading in a methane environment. Table (8) shows that the catalyst's acidity increased as the metal loading increased. This implies that the effect of the platinum clusters that are present on the surface of the ZSM-5 catalyst undermined the effects of pore channel restriction due to metal loading. The selectivity data in Figure 18 show that Pt had the lowest selectivity toward BTEX when methane was not present. However, when

methane was present, a significant increase in selectivity toward BTEX was observed. It was noted that a Pt loading of 1% gave the highest selectivity of 4.41%.

The addition of methane also had a significant impact on the formation of coke on the catalyst. The most coke was formed when 1% Pt was used. The clear increase in selectivity and increase in the amount of coke in the presence of methane indicated the coupling of methane steam reforming with furan deoxygenation in the presence of Pt.

Table 8. Bronsted acidity of pure ZSM-5 and Pt impregnated catalyst

Property	ZSM-5	1% Pt/ZSM-5	2% Pt/ZSM-5	5% Pt/ZSM-5
Bronsted acidity (mmol/g)	124.4	128.7	110.6	216.3

Ni-impregnated catalyst

The use of nickel as a steam reforming catalyst is well known [83]. Compared to noble metals, such as Ru, Rd, Pd, and Pt, Ni is far less expensive, but it can be deactivated easily due to oxidation or coke formation [102]. The activity of the Ni catalyst is related to the surface area of the Ni clusters. Having Ni particles aggregated at the pore opening or inside the pore channels can impact the functionality of the catalyst significantly. According to the BET surface area data given in Table (9), there also was a significant decrease in the surface area as the Ni loading increased. The acidity of the catalyst also increased as the metal loading increased.

The data indicated that Ni had an interesting impact on furan deoxygenation. Figure 17(B) shows that the furan conversion increased as the Ni loading increased.

When methane was co-fed with furan, a decrease in conversion was observed compared to the methane-free condition. However, the conversion increased as the metal loading increased. It was observed that 5% Ni provided the greatest furan conversion of 93.3% in the presence of methane. This effect of increased furan conversion in the presence of methane was likely due to the coupling of the methane steam reforming reaction and the furan deoxygenation reaction. Figure 18 shows that the selectivity for BTEX in a methane-free environment decreased as the metal loading values increased. When methane was co-fed with furan, the selectivity for BTEX increased significantly. The highest selectivity for the Ni catalyst was observed at 5% metal loading. The coke formation on the Ni catalyst was quite similar to the trend that was observed for BTEX selectivity.

Table 9. Bronsted acidity and surface area of pure ZSM-5 and Ni impregnated catalyst

Property	ZSM-5	1% Ni/ZSM-5	2% Ni/ZSM-5	5% Ni/ZSM-5
Bronsted acidity (mmol/g)	124.4	116.3	126.2	181.9
BET surface area (m^2/g)	266.247	259.22	251.591	240.364

Specific conclusions

The results that have been presented indicated that the levels of metal/metal oxides loadings had significant impacts on furan conversion. It was observed that Ga, Mo, and Cr, which exist in oxide form, produced decreases in furan conversion when the

impregnation level was increased from 1% to 5%. Since higher loadings can block the zeolite channels, this reduction in conversion likely can be attributed to pore interruptions. However, Pt- and Ni-loaded ZSM-5 catalysts contradicted this observation, by producing increasing conversions as the metal loadings increased. It also is clear from these data that furan conversion decreased when furan was co-fed with methane in the presence of the catalyst. Among the oxides, 5% Ga_2O_3 had the highest BTEX selectivity of 5.93%; among the metals, 1% Pt had the highest BTEX selectivity of 4.41% in a methane environment. By comparing the furan conversion data in a methane environment, it was concluded that 5% Ni-loaded ZSM-5 was the best catalyst for methane coupled deoxygenation.

CHAPTER V

KINETIC MODELING

Introduction

As opposed to thermodynamics in which systems are considered to be in equilibrium, chemical kinetics is a quantitative study of chemical systems that are changing with time. A kinetic analysis provides a relationship that describes how reaction rate is related to the reaction mechanisms that proceed through intermediates to final products. Further, such an analysis provides information concerning the relationship between reaction and macroscopic parameters, such as concentration and pressure. At a very fundamental level, reaction kinetics is a molecular-level phenomenon in which the distribution of the collision energy of the reacting molecules, the degrees of freedom of the molecules, and their respective potential energy levels determine the feasibility of a reaction [103].

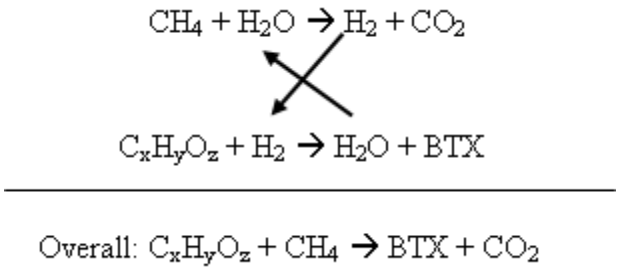

Figure 20. Proposed reaction scheme for the deoxygenation of biomass (CxHyOz) when coupled with methane

This proposed reaction scheme shown in Figure 20 consists of two reactions, in one of which methane undergoes steam reforming, while biomass oxygenates undergo the hydrodeoxygenation process in the other. To sustain the deoxygenation reaction, both reactions must occur concurrently.

Biomass pyrolysis produces about 10-20% w/w of water, which is required for the methane steam reforming reaction. It has been determined that the steam reforming reaction is catalyzed by metals, such as Ni, Ru, Rh, and Pt [104]. Since this process involves the coupling of two reactions, the catalyst must be bi-functional. Metal loaded onto acidic supports, such as ZSM-5 or γ-Al_2O_3, can act as a bi-functional catalyst. The results of the screening study reported in the previous chapter indicated that 5% Ni/ZSM-5 is one of best catalysts to catalyze this reaction.

The goals of this study was to develop an understanding of the behavior of the 5% Ni/ZSM-5 catalyst under different space velocities of the reactants and to determine the reaction order and other kinetic parameters, such as activation energies, rate constants, and the frequency factor.

Materials and methods

Furan (Sigma Aldridge), which was used as the model oxygenate in this experiment, was injected into a preheated chamber maintained at 200 ^{o}C by a syringe pump (New Era Syringe pumps, NY). The volatilized furan was mixed with a stream that contained helium and methane, as shown in Figure 21. The methane concentration was maintained at 90% v/v, and the total flow rate of the gas mixture was maintained at 35 ml/min by flow controllers. The catalytic reactor was a quartz tube that was 10 cm long and had an

OD of 6 mm; 25 mg of catalyst were used in each run. In order to approach plug-flow conditions, the ratio of the length of the catalyst bed to the size of the catalyst particles (L/d_p) was maintained in the range of 400 - 1000 [105].

The ZSM-5 catalyst ($SiO_2/Al_2O_3 = 30$, Zeolyst Corp.) was received in the form of NH_4ZSM-5, and it was used as a support. The NH_4ZSM-5 catalyst was calcined at 500 ^oC for 4 hr to transform it to HZSM-5. The 5% Ni-loaded ZSM-5 was prepared by impregnating the H-ZSM5 catalyst with nickel III nitrate hexahydrate. After the supported catalyst was impregnated with the salt solution, it was dried at 50 ^oC for 4 hr and calcined at 500 ^oC for another 4 hr. The calcined nickel catalyst was reduced in a H_2 stream (50 ml/min) for 2 hr at 500 ^oC before it was used.

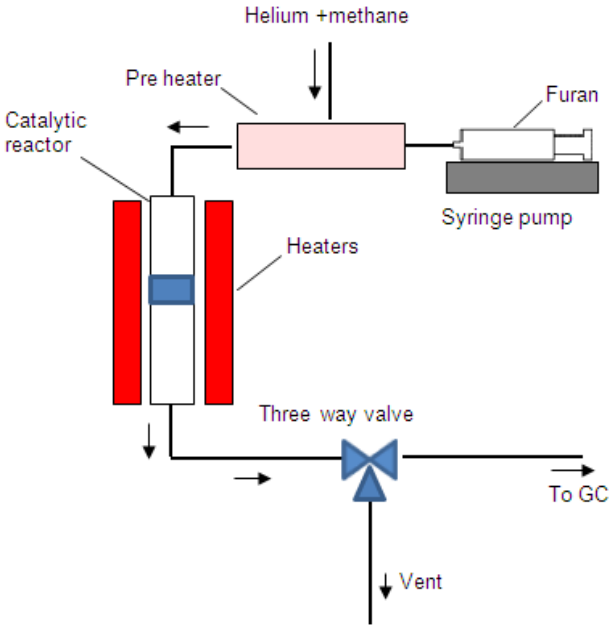

Figure 21. Schematic diagram of the reactor system used in the study

GC/MS analyses were performed using an Agilent 7890 GC equipped with a 5890 mass detector (Agilent Technologies, Santa Clara, CA, USA). The column used for the GC/MS analyses was CP-Sil PONA CB (100 m, 0.25-mm OD, 0.5-μm ID). The GC was equipped with a gas sampling valve to inject the samples to the GC. The gas samples were collected 5 min after the reaction began to allow the system to stabilize. Different weight hourly space velocities were selected by varying the catalyst amount (15, 25, 30, 35, and45 mg). Coke deposition on the catalyst was quantified by a thermo-gravimetric analyzer (TGA Q50) (TA Instruments). Preliminary tests were conducted to check the catalyst's deactivation, and no sign of deactivation was observed during sample collection.

The actual reactions that take place during furan deoxygenation are complex and involve decarbonylation, Diels-Alder condensation, dehydration, and oligomerization [95]. In order to simplify the system, the overall reaction was modeled by lumping products together as shown in Equation (26) in which A, B, and C represent furan, methane, and hydrocarbons, respectively. Using the power law model, the rate of disappearance of furan was represented as shown in Equation (27), in which 'k' represents the rate constant, and α and β are the orders of the reaction.

$$A+B \longrightarrow C \tag{26}$$

$$-d[A]/dt = k\,[A]^{\alpha}\,[B]^{\beta} \tag{27}$$

$$k\,[B]^{\beta} = k^{1} \tag{28}$$

$$-d[A]/dt = k^{1}.\,[A]^{\alpha} \tag{29}$$

$$\ln[-d[A]/dt] = \ln[k^1] + \alpha.\ln[A] \quad (30)$$

$$t= (1/k^1).\ \{[A_o]^{(1-\alpha)}-[A]^{(1-\alpha)}\}/(1-\alpha) \quad (31)$$

By using the method of excess, Equation (27) can be simplified since the methane concentration [B] was selected to be significantly large. Therefore, a new rate constant, k', can be defined as given by Equation (28). The new rate law given in Equation (29) can be transformed into linear form as given by Equation (30), where α and k^1 can be estimated by plotting the straight line, ln[-d[A]/dt] vs. ln[A], as given in Figure 22.

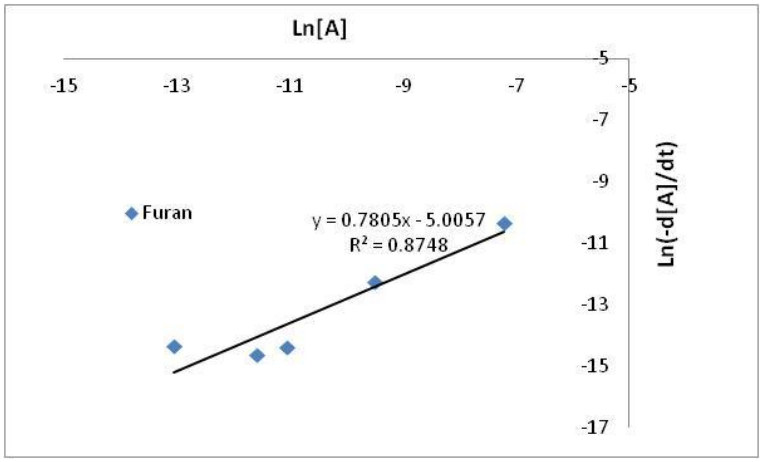

Figure 22. Graphical representation of ln[-d[A]/dt] vs. ln[A]

In order to get a more accurate estimation of α and k^1, a regression formula can be derived from Equation (29) as given in Equation (31), where 't' represents the time, and $[A_o]$ represents the concentration of furan at the onset of the reaction. Regression analysis was performed using Polymath 5.1, with the initial estimates obtained from the

graphical method, where $\alpha = 0.7805$ and $k^1 = 0.0067$. The parameter values in the model were determined by the built-in Levenberg-Marquardt algorithm, and the new values that were obtained were $\alpha = 0.90058$ and $k^1 = 0.0218$. The reaction order of methane, 'β', was determined using the same procedure subsequent to the estimation of 'α'. In this procedure, we again assumed the method of excess in which we assumed the furan concentration was very high and constant. The experiment was conducted as a full-factorial design with three replicates. The results were analyzed at $\alpha = 0.05$ significance level using Design-Expert software (Stat-Ease, Inc. Minneapolis, MN, USA).

Results and discussion

Methane steam reforming

Nickel is the most extensively used catalyst in steam reforming processes. Despite its extensive use, it is less active than noble metals and is prone to deactivation due to coking [106]. Studies conducted by Xu and Froment on Ni catalysts indicated that the rate determining reactions were those between adsorbed oxygen and carbon intermediates [107]. Several other research groups also have proposed their own mechanisms for methane steam reforming. For example, Rostrup-Nielson proposed a four-step mechanism that challenged Xu and Froment's model, and they proposed that methane dissociation does not proceed via an adsorbed precursor [108]. Due to the complex nature of these mechanisms, it is difficult to use such reaction steps to determine the rate parameters. Wei and Iglesia conducted in-depth studies of CH_4 activation and concluded that reaction rate of methane steam reforming was proportional

to partial pressure of CH_4 and co-reactants [109]. According to the literature, DFT studies conducted on C-H bond activation on Ni catalyst have indicated that the activation energy is in the range of 85 -100 kJ/mol [106]. Chemical kinetics studies conducted on the methane steam reforming reaction have indicated the activation energy of the reaction was around 96.1 kJ/mol and that the frequency factor was 7.26×10^7 s^{-1} [106].

Since both methane and water are reactants in the methane steam reforming reaction, studies have been conducted to determine the optimum H_2O/CH_4 ratio for the reforming reaction. Hoang et al. concluded that the reforming efficiency increased as temperature increased when the H_2O/CH_4 ratio was in the range of 2-5 [110]. When the H_2O/CH_4 ratio was greater than 5, the reforming efficiency decreased for temperatures greater than800 ^oC. The optimum values that can be found for the H_2O/CH_4 ratio are in the range of 3-4 when the temperature is in the range of 700 - 800 ^oC [110].

Furan deoxygenation

The deoxygenation of furan proceeds through three major reaction pathways, i.e., dehydration, decarbonylation, and decarboxylation. The deoxygenation of furan has been studied by several researchers using H-ZSM-5 catalyst, which has strong Bronsted acidity, hydrophobicity, and shape selectivity. According to Grandmaison et al., the opening of the furan ring begins in the dehydration step, and succindialdehyde is formed inside the pores of the ZSM-5 catalyst [89]. Huber et al. identified two pathways for forming allene and benzofuran [94]. Allene was formed through the decarbonylation reaction, and benzofuran was a product of the Diels-Alder condensation reaction. Further

progression of these chemical pathways would produce heavier aromatics and olefins. According to experimental observations, it has been reported that the most selective form of carbon is carbon monoxide in the product spectrum. This is an indication that the decarbonylation pathway is dominant in the deoxygenation process. Recent studies on deoxygenation have shown that the space velocity also is an important parameter that has a significant impact on furan conversion. Higher furan conversion has been observed for low space velocities (WHSV = 1.95 h^{-1}) [120]. Kraushaar et al. studied the hydrodeoxygenation of furan over HZSM-5 and Pt-ZSM-5 at 400 ^{o}C with low space velocities (WHSV = 0.5h^{-1}) and indicated that low H/C ratios of furan can be increased to higher values by adding hydrogen. It has been reported that the presence of Pt on ZSM-5 favors the hydrogenation process, while the presence of HZSM-5 promotes the Diels-Alder condensation process [89]. Studies also have been conducted using Al_2O_3-based catalysts, such as $CoMo/Al_2O_3$.Comparison of the reduced and the sulfide forms of $CoMo/Al_2O_3$ indicated that the sulfide form provided double the conversion for hydrodeoxygenation provided by the reduced catalyst. Thermodynamic equilibrium calculations on hydrodeoxygenation showed that the furan ring was hydrogenated completely to terahydrofuran before the oxygen elimination took place [111].

Methane coupled deoxygenation

Figure 23 shows the carbon selectivity of BTEX in the presence of methane over the 5% Ni/ZSM-5 catalyst as a function of space velocity. The selectivity for benzene (which is a major product of the deoxygenation process) was at its highest value at700 ^{o}C. This further indicated that the carbon selectivity reached a maximum of 2.54% at WHSV =

42.69 h^{-1} at700 ^{o}C. The benzene selectivity reached a maximum at WHSV = 42.69 h^{-1} at 700 ^{o}C, confirming that higher temperatures favor direct methane activation and coupling.

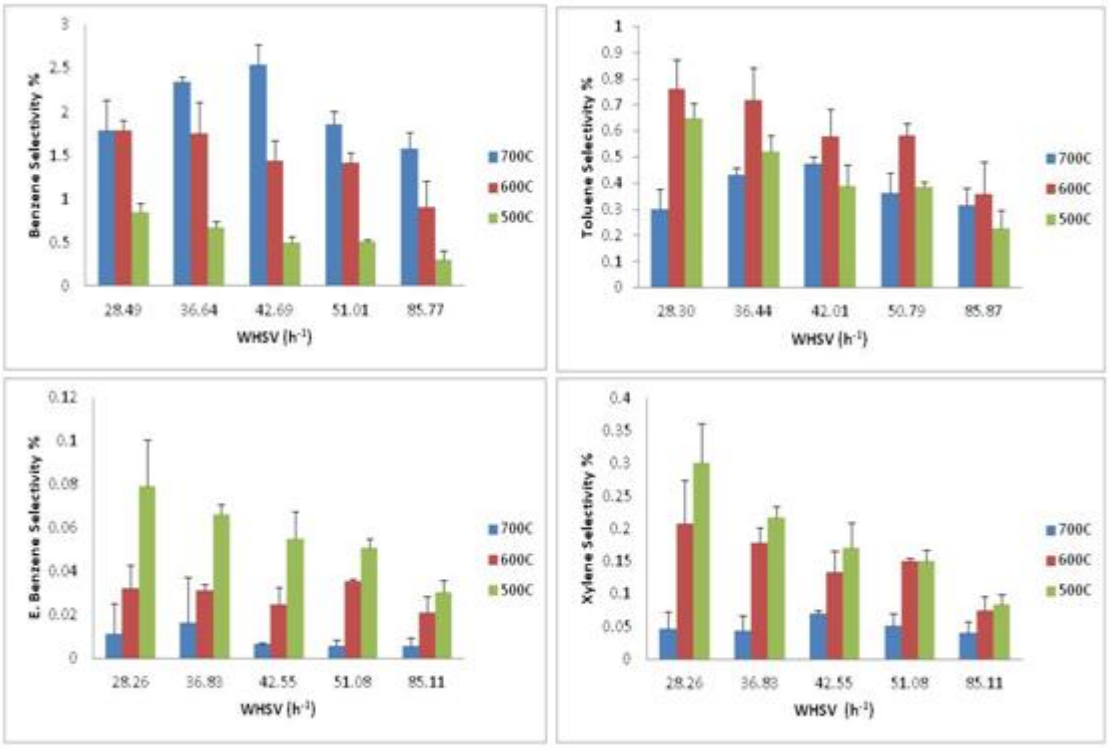

Figure 23. Selectivity for benzene, toluene, ethylbenzene, and xylene (BTEX) for various weight hourly space velocities (WHSVs) (n=3, α=0.05)

According to Figure 24 the above observation was justified further due to the tendency for furan to undergo conversion as the WHSV values increased. The carbon selectivity for toluene is at its highest value at 600 ^{o}C, and increasing WHSV decreases the toluene selectivity. The highest carbon selectivity for toluene was 0.76% at WHSV = 28.3h^{-1}. The methylated aromatic products, such as toluene, ethylbenzene, and xylenes,

have the highest carbon selectivity at WHSV = 28.3h^{-1} at which the reactants stay in the catalyst for a longer time. Therefore, this implies that long residence times aid the methylation of the aromatic ring.

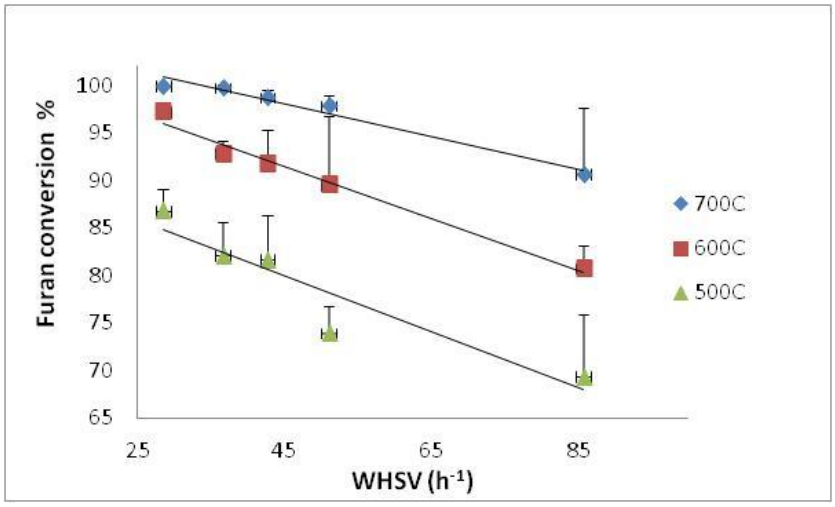

Figure 24. Furan conversion over 5% Ni/ZSM-5 in the presence of methane at different weight hourly space velocities (n=3, α=0.05)

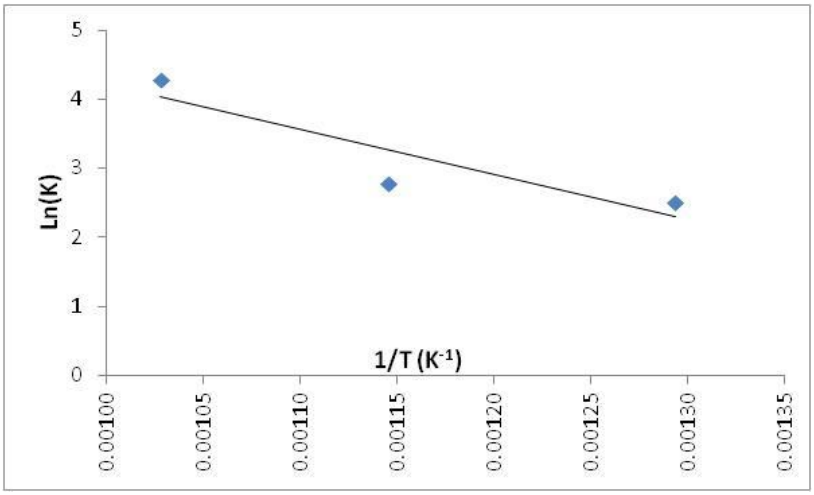

Figure 25. Arrhenius plot for furan deoxygenation in the presence of methane over Ni/ZSM-5

While the carbon selectivity of benzene was higher at700 ^{o}C, the selectivity for methylated products, such as ethyl benzene and xylene, were higher at500 ^{o}C. The highest carbon selectivity for ethyl benzene and xylene reported in this study were 0.079% and 0.3%, respectively at WHSV = 28.3h^{-1} and500 ^{o}C. At any given temperature, the product selectivity decreased according to the following order: CO > CO_2 > benzene > toluene > xylene > ethyl benzene. Since carbon selectivity for CO was higher than the rest of the products, it can be expected that the decarbonylation step is the predominant step in the deoxygenation process.

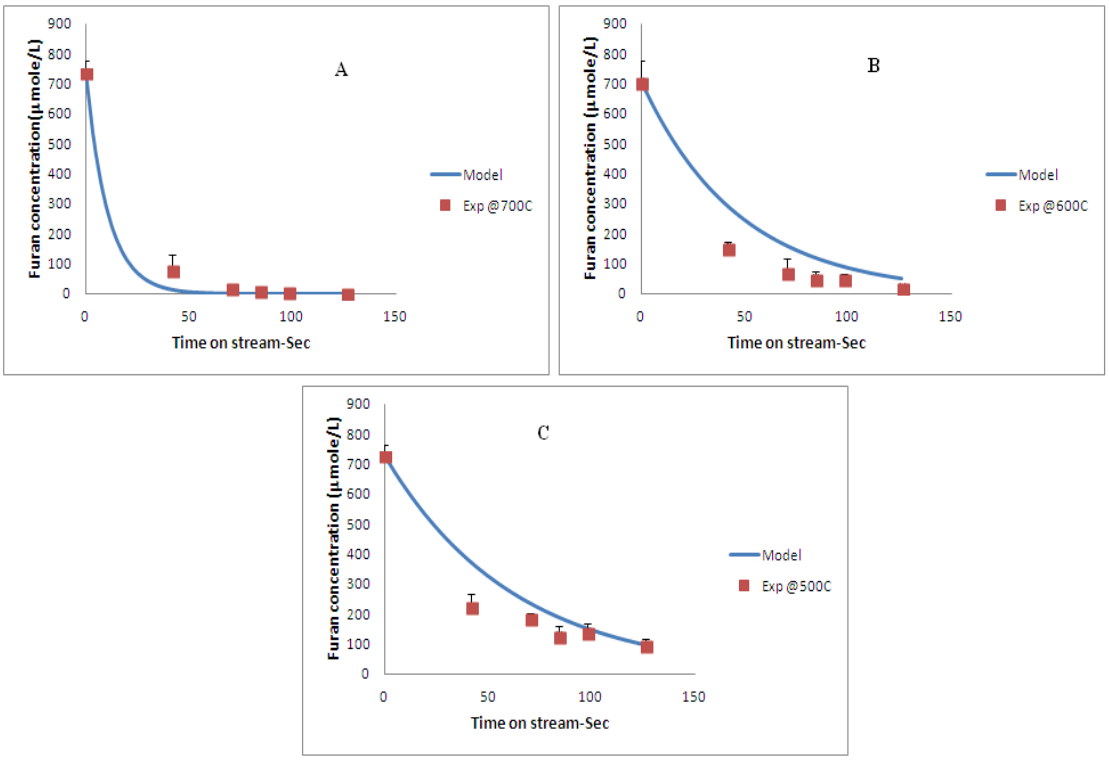

Figure 26. Comparison of predicted and experimental values of furan concentrations at different temperatures

According to the power law model, the rate equation for furan deoxygenation in the presence of methane can be written as shown in Equation (32). The rate constant 'k' in Equation (32) varies with temperature, as shown in the Arrhenius plot in Figure 25. The values of 'k' at various, specific reaction temperatures were 73.4 $l^2m^{-2}s^{-1}$, 16.33 $l^2m^{-2}s^{-1}$, and 12.32 $l^2m^{-2}s^{-1}$ at 700, 600, and 500 ^oC, respectively. The calculated kinetic values in this study for 5% Ni/ZSM-5 were 54.108 kJ.mol for the activation energy and 4.53 x 10^4 $l^2m^{-2}s^{-1}$ for the pre-exponential factor.

$$d[Furan]/dt = k.\ [Furan].\ [Methane]^2 \quad (32)$$

Figure 26 shows the changes in the concentration of furan with time at different temperatures calculated by the model rate equation. Figure 26 indicates that the predicted values were in good agreement with the experimental data at 700 ^oC.

Specific conclusions

The carbon selectivities of benzene, toluene, ethyl benzene, and xylene were affected significantly by temperature. Higher temperatures favored the selectivity for benzene, while lower temperatures favored the selectivity for ethyl benzene and xylene. Benzene reported the highest carbon selectivity of 2.54% at WHSV = 42.69 h^{-1} at700 ^oC.

According to the kinetic study, the rate of change in the concentration of furan was first order with respect to the methane concentration and second order with respect to the furan concentration. The estimated kinetic parameters were 54.108 kJ.mol for the activation energy and 4.53 x 10^4 $l^2m^{-2}s^{-1}$ for the pre-exponential factor.

CHAPTER VI

CATALYST DEACTIVATION

Introduction

The use of catalysts is the most effective way to upgrade biomass pyrolysis products; however, catalyst deactivation during the process is a critical challenge; in fact, it is a major technical, economic, and environmental issue in industrial chemical processes [112, 113]. Therefore, a study of catalyst deactivation is of primary importance in the development of catalytic processes. This study focused particularly on the deactivation of the Ni/ZSM-5 catalyst when model oxygenate, furan, was deoxygenated to form hydrocarbons in the presence of methane. As mentioned in previous chapters, methane coupled deoxygenation involves the amalgamation of two separate reactions. Therefore, both reactions can have significant impacts on the deactivation of the catalyst. The overall reaction for this process can be represented as a single reaction as shown in Equation (33).

$$3C_4H_4O + CH_4 \longrightarrow 2C_6H_6 + CO + 2H_2O \quad (33)$$

Materials and methods

A syringe pump (New Era Syringe pumps, NY) was used to inject furan (Sigma Aldridge), i.e., the model oxygenate in this experiment, into a preheated chamber maintained at 200 ^{o}C. The volatilized furan was mixed with a steam that contained helium and methane, as shown in Figure 27. The methane concentration was maintained at 90% v/v, and the total flow rate of the gas mixture was maintained at 35 ml/min by

flow controllers. The catalytic reactor was a10 cm long 6 mm OD quartz tube and 25 mg of catalyst was used in each run. In order to approach plug flow conditions, the ratio between the length of the catalyst bed and the catalyst's particle size (L/d_p) was maintained in the range of 400 - 1000 [105]. Catalyst regeneration and reduction also were conducted in the same reactor. First, valves V1 and V2 were kept closed, and V3 was kept open to the reactor. When the catalyst was being regenerated, V1was open, and V2 was closed. Valve V3 was opened to the vent position. In the regeneration mode, the V1 was closed, V2 was open, and V3 was in the vent position. The experiment was conducted as a full-factorial design with three replicates. The results were analyzed at α = 0.05 significance level using Design-Expert software (Stat-Ease, Inc. Minneapolis, MN, USA).

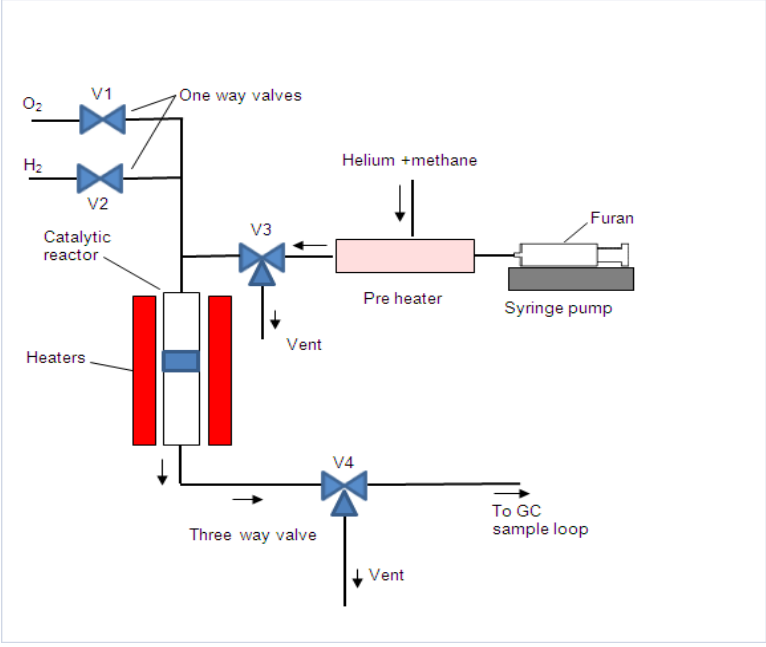

Figure 27. Line diagram of the reactor system used in the study

The ZSM-5 catalyst (SiO_2/Al_2O_3=30, Zeolyst Corp.) was used as a support and was received in the form of NH_4ZSM-5. The NH_4ZSM-5 catalyst was calcined at 500 ^oC for 4hrs to transform it to HZSM-5. The 5%Ni loaded ZSM-5 was prepared by impregnating nickel III nitrate hexa hydrate on H-ZSM5 catalyst. After impregnating with the salt solution, the supported catalyst was dried at 50 ^oC for 4 hrs and calcined at 500 ^oC for another 4 hrs. Calcined Nickel catalyst was reduced in a H_2 stream (50ml/min) for 2hrs at 500 ^oC before being used.

The major types of deactivation that are relevant to this study are poisoning, fouling, and sintering [114]. Poisoning, which is the irreversible chemisorption of contaminants or undesired products, is considered a major type of deactivation when transition metals, such as Fe, Rh, Ni, and Pt are used [115]. Specifically, the presence of CO and high molecular weight polyaromatic compounds in the reaction environment can result in catalyst deactivation by poisoning. In this process, both the steam reforming and deoxygenation reactions produced significant amounts of CO. According to work done by Huber et al. on furan deoxygenation, CO was a major product of the decarbonylation of furan [88].

Results and discussion

Extensive work done by Froment et al. on the steam reforming reaction indicated that catalyst deactivation by irreversible adsorption of CH_x species occurs in an oxygenate-free environment in which H- abstraction proceeds in a series of steps [105]. Figure 28 shows the CH_2- moieties that are formed as a result of methane activation and that promote coke formation because they can form strong bond on the surface of the Ni. In

addition to the CH_x species, the deposition of solid carbon also can deactivate the catalyst.

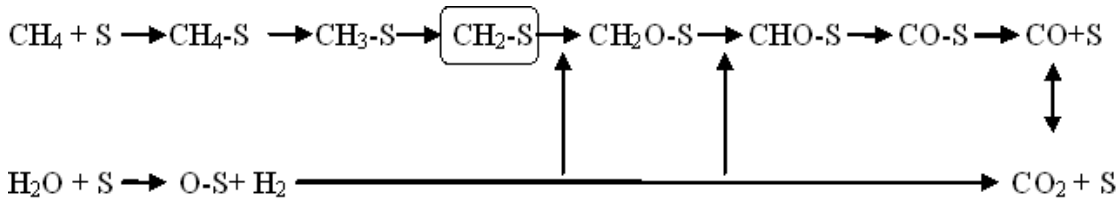

Figure 28. Simplified reaction scheme for methane reforming at the active catalyst site

Table 10. Gibbs free energy for several possible carbon-forming reactions at 600 ^{o}C [95]

Reaction	ΔG_{rxn} (kJ/mol)	No.
$CH_4 \longrightarrow C + 2H_2$	22.7	1
$2CO \longrightarrow C + CO_2$	-66.2	2
$C_4H_4O \longrightarrow C_2H_4 + CO + C$	-269	3
$2C_4H_4O \longrightarrow C_3H_6 + 2CO + H_2 + 3C$	-380	4
$3C_4H_4O \longrightarrow C_7H_8 + 3CO + 2H_2 + 2C$	-528	5
$3C_4H_4O \longrightarrow C_8H_{10} + 3CO + C + H_2$	-464	6
$3C_4H_4O \longrightarrow C_{10}H_8 + 4CO + 4H_2 + 2C$	-615	7
$C_4H_4O \longrightarrow 4C + H_2O + H_2$	-280	8

According to the reactions given in Table (10), methane dehydrogenation to form solid carbon is not thermodynamically favorable, but CO conversion to solid carbon is

significantly favorable. Reactions (3) trough (8) in Table (10) depict carbon formation from furan. According to the thermodynamics, the formation of polyaromatic hydrocarbons is more highly favorable than the formation of C_2H_4. Therefore, deactivation of the catalyst due to the deposition of solid carbon during furan conversion is most likely to occur through reactions in which polyaromatic hydrocarbons are formed.

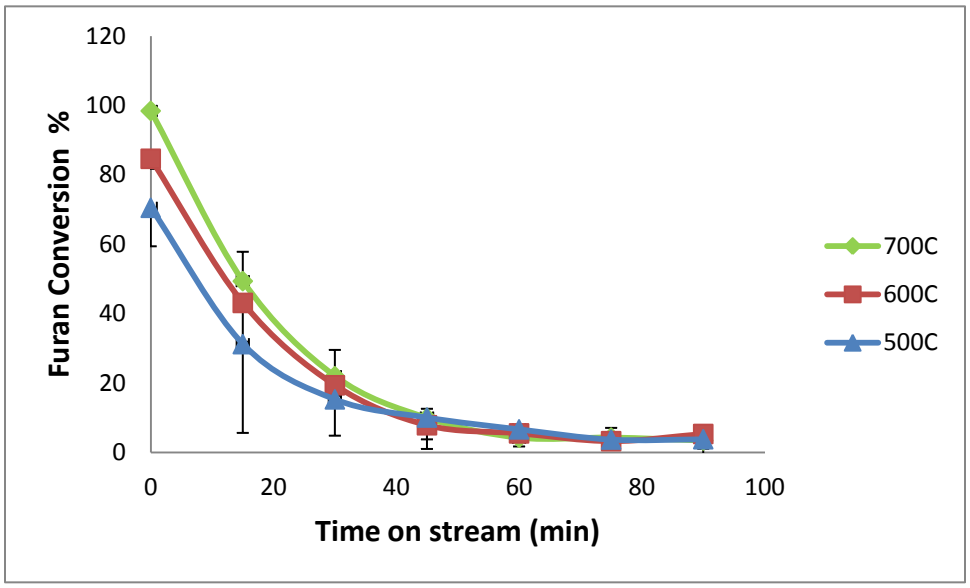

Figure 29. Change in furan conversion as a function of time on stream (n=3, α=0.05)

The results of this study indicated that furan conversion dropped exponentially with time due to catalyst deactivation. Figure 29 shows that furan conversions at different temperatures were significantly different at the beginning of the reaction. The effect of temperature on deactivation became negligible as the reaction time increased.

After 45 minutes of reaction time, the catalyst was deactivated completely, and furan conversion reached a steady state.

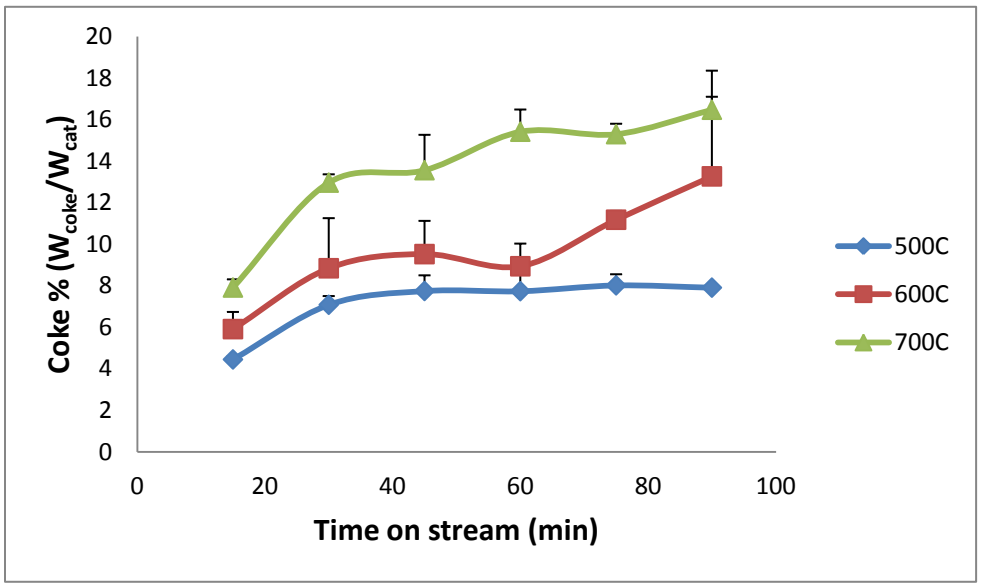

Figure 30. Yield of carbon (coke) as a function of time on stream (n=3, α=0.05)

Figure 30 shows the increases in the coke percentage as the reaction time increases. It also shows that the maximum coke yield was 8.0±0.5% (w/w) at the lower temperature of 500 ^{o}C and that the yield reached steady state after 40 min of reaction time. Coke yield increased as the temperature increased, and the maximum coke yield of 16.5±1.9% (w/w) occurred at the highest temperature (700 ^{o}C). Deposition of carbon or coke on the porous catalyst, which blocks the active sites, is called fouling. The steady state behavior that was clearly visible at 500 ^{o}C after 45 minutes was due mainly to the pores being blocked by carbon. Heavy fouling was observed as the temperature increased due to additional carbon deposition on the surface of the catalyst.

The literature suggests that continuous carbon deposition results in the formation of whiskers that caries Ni at the top of the stem [105]. This results in the disintegration of the catalyst particles and plugs the reactor's void spaces. According to Batholomew et al., low temperatures during the steam reforming reaction process produced more condensed polymer, whereas higher temperatures yielded graphite carbon. The empirical Voorhies' relationship given in Table (11) provides a reasonable approximation of the fouling that occurs in a porous medium [115, 116]. In gas oil cracking, typically the value of 'n' is $0.5 < n < 1$ [115]. According to the values given in Table (11), the fouling parameters vary depending on the temperature, and, at700 ^{o}C, n = 0.51, which indicates that the deactivation was affected by diffusion.

A catalyst that has been deactivated must be reactivated by burning off the carbon and reducing the active metal sites. According to the catalyst regeneration data in Figure 31, the activity of the catalyst is affected by the temperature of the reaction. At 500 ^{o}C, it is apparent that the deactivated catalysts were restored to their original conditions several times. However, this behavior changed completely when the catalyst's temperature was maintained at600 or 700 ^{o}C. At these temperatures, thermally-induced deactivation was observed. Therefore, the loss in catalyst activity in the regeneration cycles was related to sintering and structural disintegration. Such losses cannot be restored by the simple regeneration process used in this study.

Sintering is a complex phenomenon that occurs at high reaction temperatures, and it is said to be accelerated by the presence of water vapor [117]. Figure 31 shows that the furan conversion after the regeneration step at 600 ^{o}C decreased to 37.8±8.8%,

while, at700 ^{o}C, it decreased to 50.1±5.1%. This increase in conversion at 700 ^{o}C was due to the effect of temperature on furan conversion kinetics.

Table 11. Fouling parameters from Voorhies' equation

$C = A * t^{n}$		
T (^{o}C)	A	n
500	0.529	0.32
600	0.112	0.76
700	0.414	0.52

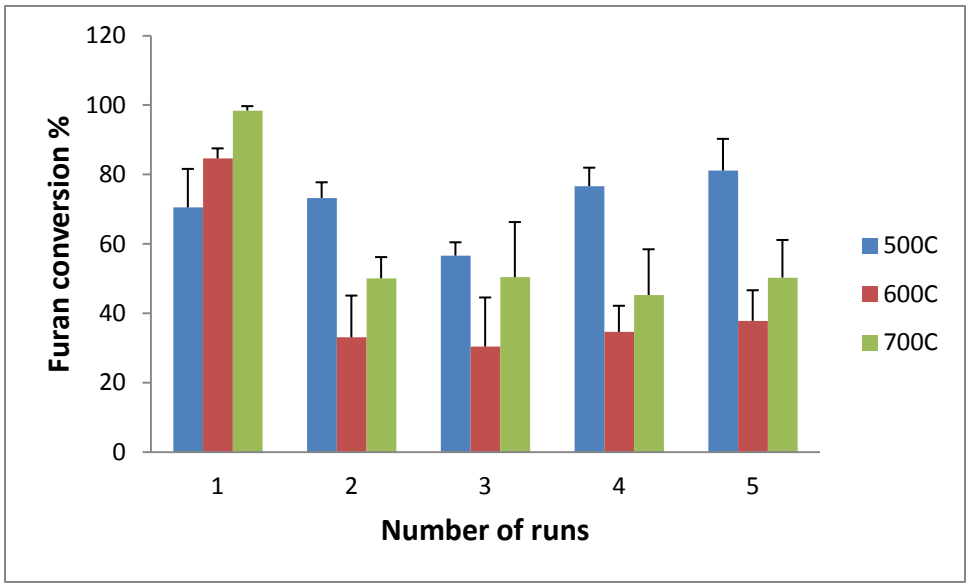

Figure 31. Furan conversion as a function of catalyst regeneration cycles (n=3, α=0.05)

Specific conclusions

Poisoning, fouling, and sintering are three intrinsic mechanisms of catalyst deactivation that were relevant in this study. Poisoning and thermal degradation are generally

irreversible, while fouling by solid carbon or polyaromatics can be reversed easily. Carbon deposition and coking may be minimized by improving the mass transport in the catalyst bed. Sintering can be avoided by selecting lower operational temperatures. After 40 min of reaction time, the catalyst's activity decreased significantly, and it had to be regenerated. At 500 ^{o}C, we were able to restore the catalyst's activity to its original level, but, at temperatures greater than600 ^{o}C, sintering prevented the complete restoration of the catalyst's activity.

CHAPTER VII

CHARACTERIZATION OF BIO-OIL PRODUCED IN A BATCH REACTOR

Introduction

With the increasing concerns over the sustainability of petrochemical fuels, biomass-based fuels have shown unprecedented promise for meeting the world's future energy demand [79, 118, 119]. Among biomass thermal conversion processes, pyrolysis is of great interest, and it has been studied extensively for use in producing liquid biofuels [120]. Depending on the heating rate used, four modes of pyrolysis can be identified. They are fast pyrolysis, intermediate pyrolysis, torrefaction, and carbonization. Fast pyrolysis involves very high heating rates (10^3-10^5 C^o/s) and short vapor residence times and can produce 70-80 wt% of high quality bio-oil [121]. The reactions involved in pyrolysis can be classified generally into two categories, i.e., dehydration and fragmentation. Typically, dehydration is the dominant reaction at lower temperatures (< 300 ^oC) at which reduction in molecular weight and the evolution of H_2O, CO, and CO_2 are observed. The fragmentation reaction is dominant at higher temperatures (> 300 ^oC) at which biomass depolymerization to anhydrous sugars, such as levoglucosan, are observed [120]. As discussed in Chapter I, raw bio-oil is a complex mixture of hundreds of organic compounds, including carboxylic acids, aldehydes, ketones, alcohols, furfural, and phenols. Since these components of bio-oil exist at low concentrations, it is significantly challenging to separate them into individual chemicals. By using upgrading processes, such as hydroprocessing or catalytic cracking, bio-oil can be converted to a

fraction that is rich in hydrocarbons and compatible with petroleum crude. Several catalysts have been tested for upgrading bio-oil, including ZSM-5, H-beta, HY, MCM-41, MCM-48, and SBA-15. It has been reported that acidic ZSM-5 particularly has a higher selectivity toward aromatic products during the deoxygenation process [122]. It was discussed in detail in the previous chapters that methane can be used as a substitute for hydrogen [94]. This study was focused on determining the effect of the presence of methane in the deoxygenation medium on the production of bio-oil from the pyrolysis of cellulose and sorghum in the presence of a Ni/ZSM-5 catalyst.

Materials and methods

Sweet sorghum was used as the biomass, and cellulose was purchased from Sigma Aldridge and used as received. For each experiment, 25 g of sample were used in a batch reactor. The ZSM-5 catalyst ($SiO_2/Al_2O_3 = 30$, Zeolyst Corp.) was used as a support, and it was received in the form of NH_4ZSM-5. The NH_4ZSM-5 catalyst was calcined at 500 ^oC for 4 hr to transform it into HZSM-5. The 5% Ni-loaded ZSM-5 was prepared by impregnating the H-ZSM5 catalyst with nickel III nitrate hexahydrate. After being impregnated with the salt solution, the supported catalyst was dried at 50 ^oC for 4 hr and calcined at 500 ^oC for another 4 hr. The calcined nickel catalyst was reduced in a H_2 stream (50 ml/min) for 2 hr at 500 ^oC before being used.

For the catalytic experiments, 2.5 g of catalyst were used in the reactor. In order to approach plug flow conditions, the ratio between the length of the catalyst bed and the size of the catalyst particles (L/d_p) was maintained in the range of 400 - 1000 [105]. The batch reactor, catalytic reactor, condenser, and the cryogenic trap were connected as

shown in Figure 32. The system was purged with nitrogen to maintain an inert atmosphere for the pyrolysis process, and the flow was maintained at900 ml/min. The pyrolysis reactor and the catalytic reactors were maintained at600 ^{o}C. The experiment was designed as a factorial design with two factors being the substrates (cellulose, sorghum) and the reaction conditions (with and without methane). The pyrolysis products were quenched by using a liquid nitrogen cold trap. The organics and water were separated by using a solvent extraction method using dichloromethane as the solvent. The aqueous phase was analyzed by an HPLC system. The solvent phase was subjected to vacuum distillation to separate the organic phase for further analysis.

(a)

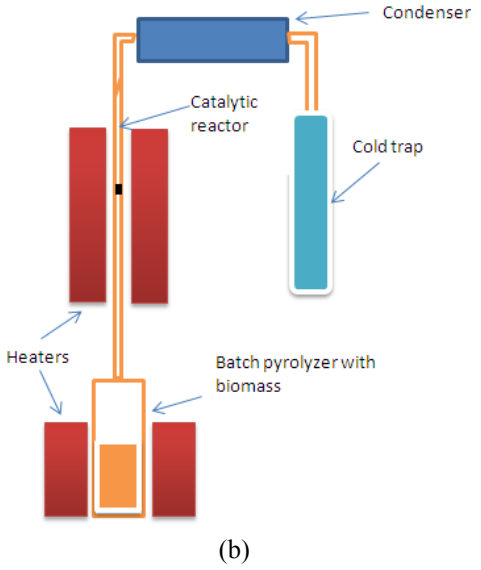

(b)

Figure 32. Experimental setup: (a) full reactor system; (b) schematic of the reactor system

The effective H:C ratio was calculated from the mole values of C, H, O, N, and S, as given by Equation (34). The high heating value (HHV) of the bio-oil was predicted by the empirical equation presented by Francis and Lloyd and given by Equation (35), in which C, H, N, S, and O represent the weight percentages of the corresponding elements from the elemental analysis [123].

$$H:C = (H-2O-3N-2S)/C \quad (34)$$

$$HHV = 357.8C + 1135.6H + 54.9N + 119.5S – 85.4O – 974 \quad (35)$$

The NMR spectra were obtained on an 11.7 T Varian Inova 500 spectrometer operating at 500-MHz proton frequency. In order to avoid solvent interference, deuterated dichloromethane (CD_2Cl_2) was used to extract the bio-oil. The experiment was conducted as a complete randomized design with three replicates. The results were analyzed using one way ANOVA at $\alpha = 0.05$ significance level using Design-Expert software (Stat-Ease, Inc. Minneapolis, MN, USA).

Results and discussion

As described before, the objective of this study was to produce bio-oil using cellulose and sorghum in a batch reactor. The temperature profile of the batch reactor indicated that the fast pyrolysis conditions were not met. The heating rate was within the slow pyrolysis regime in which carburization takes place.

Cellulose pyrolysis

Cellulose is a major component of biomass, so there is a close similarity between the products produced from the pyrolysis of cellulose and biomass. The slow pyrolysis of cellulose involves the reduction of the degree of polymerization, formation of free radicals, elimination of water, formation of carbonyl and carboxyl groups, and the evolution of non-condensable gases, such as CO and CO_2, and char residue.

Table 12. Product yield from the pyrolysis of cellulose and sorghum

Source	Methane	Biomass	Cat wt.	pH	Char %	Coke %	Bio-oil%	Gas %
Cellulose	no	25.00	0.00	1.86	20.60	0.00	5.56	32.92
	no	25.00	2.50	1.98	19.18	1.22	2.90	57.17
	yes	25.00	2.50	2.10	19.67	0.52	1.54	56.76
Sorghum	no	25.00	0.00	3.13	46.59	0.00	2.21	32.23
	no	25.00	2.50	3.03	43.39	0.71	1.89	38.64
	yes	25.00	2.50	4.40	41.91	0.60	1.19	37.20

According to the data in Table (12) for the pyrolysis of cellulose, the pH of the aqueous fraction indicated the significant presence of carboxylic acid groups. When methane was used in the medium, there was an increase in the pH, indicating that the acidity had decreased slightly in the medium. This was evidence of the occurrence of the decarboxylation reaction in the presence of methane. Further, it showed that the yield of bio-oil decreased from 5.56% for non-catalytic pyrolysis to 1.54% for the methane coupled pyrolysis conditions. This decrease in the yield can be attributed to the presence of the catalyst in the reactor with the catalyst bed acting as a restriction to the flow of

vapor. Further, the catalyst caused a significant increase in the quantity non-condensable gases.

Table 13. Effective H:C ratio and the HHV for the pyrolysis of cellulose and sorghum

Source	Methane	Biomass	Cat wt.	H:C	HHV (kJ/kg)
Cellulose	no	25.00	0.00	0.49	33811.25
	no	25.00	2.50	0.48	34949.41
	yes	25.00	2.50	0.53	35893.1
Sorghum	no	25.00	0.00	0.47	33476.08
	no	25.00	2.50	0.51	34534.85
	yes	25.00	2.50	0.53	36532.81

The Table (13) indicates that the H/C and HHV values of bio-oil were the highest when methane was used with the Ni/ZSM-5 catalyst. It was proven in a previous study that, when biomass pyrolysis occurs in the presence of methane and the Ni/ZSM-5 catalyst, H_2 is generated in the medium as a result of the methane steam reforming reaction. Therefore, the deoxygenation medium becomes hydrogen rich and contributes to the hydrodeoxygenation reaction. This explanation was validated further by the data in Figure 33. These data compare the elemental composition of bio-oil produced at different process conditions.

Figure 33 shows that the amount of carbon present in bio-oil increased when the process was conducted in the presence of methane. The highest quality bio-oil obtained in cellulose pyrolysis was produced when methane was coupled with the deoxygenation process in the presence of the Ni/ZSM-5 catalyst.

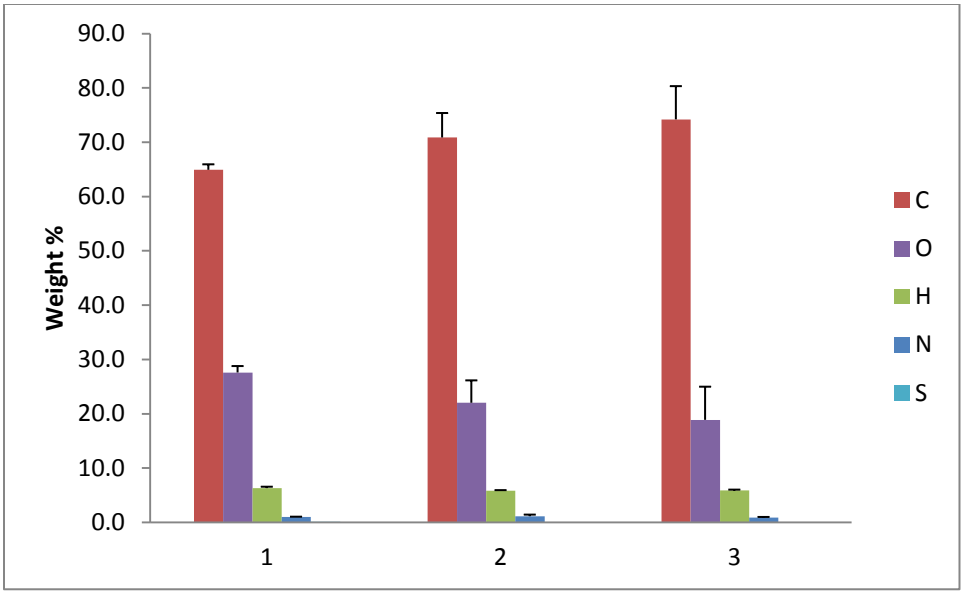

Figure 33. Elemental composition of bio-oil produced from cellulose: 1) raw bio-oil; 2) bio-oil with catalytic pyrolysis; 3)bio-oil with catalytic pyrolysis in the presence of methane (n=3, α=0.05)

Sorghum pyrolysis

Figure 34 shows the ^{1}H NMR spectrum for (A) raw bio-oil without further processing and (B) bio-oil produced in the presence of methane. Since bio-oil is a collection of several different organic compounds, the chemical shifts of the peaks are not straightforward. However, by examining specific regions, such as 0.5-1.5 ppm, 1.5-3.0 ppm, 3.0-4.4 ppm, 4.4-6.0 ppm, and 6.0-8.5 ppm, it is possible to get a good idea of the compositional changes [124]. The region with the chemical shift of 0.5-1.5 ppm represents protons that are attached to aliphatic carbon. According to the spectrum, the upgraded bio-oil had a slight increase in aliphatic protons. The region in which the chemical shift of 1.5-3.0 ppm occurred represents protons on aliphatic carbon that is bonded to C=C. According to the spectrum, both the raw bio-oil and the upgraded bio-

oil are rich in aliphatic protons, implying the presence of aromatic and olefinic compounds. The region with the chemical shift of 3.0-4.4 ppm represents protons on carbon atoms next to aliphatic alcohols or ethers. The chemical shift from 4.4-6.0 ppm represents protons from aromatic ether. Comparing the two spectra showed that there were no significant peaks present in the region from3.0-6.0 ppm. Protons from the aromatic compounds or protons connected to heteroaromatic compounds that contained O and N are represented in the region6.0-8.5 ppm. Both spectra indicate that aromatic structures are present in bio-oil [124].

The information in Table (12) indicates that the bio-oil produced from sorghum was less acidic than that produced from cellulose. As was the case for cellulose, liquids derived from the pyrolysis of sorghum also increased the pH of the raw bio-oil from 3.13 to 4.40 for upgraded bio-oil.

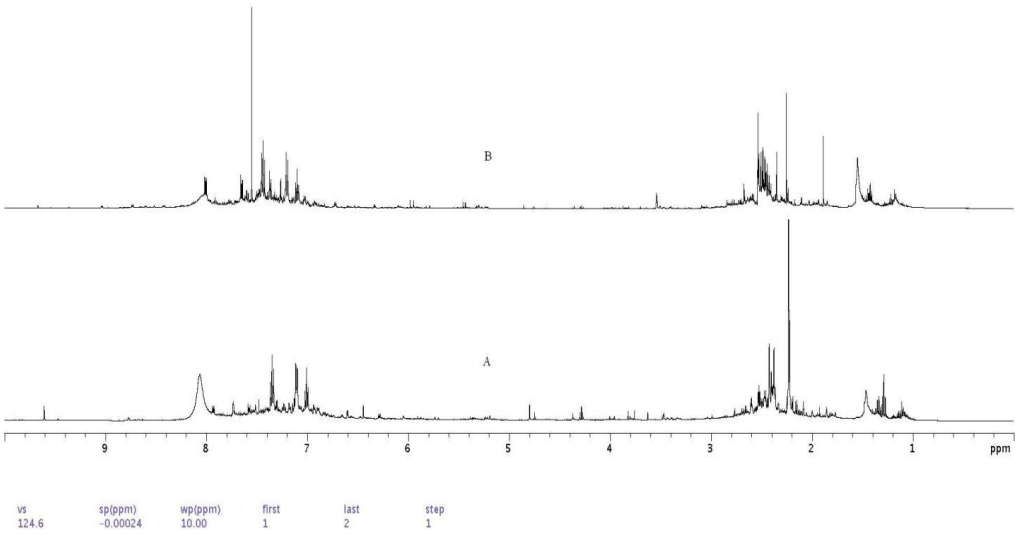

Figure 34. Proton NMR spectra: (A) raw bio-oil; (B) upgraded bio-oil produced from sorghum

The relatively higher pH values for the liquids derived from sorghum implied that the carboxylic acid fraction was lower than that for liquids derived from cellulose. The char yield for sorghum was somewhat higher than that for cellulose. This increase was mainly due to the presence of the ash component. However, it is interesting to observe that, when upgrading biomass oxygenates with the Ni/ZSM-5 catalyst and methane, the char yield decreased. The lowest char yield of 41.91% was reported when methane was coupled with the deoxygenation process. The hydrogen-rich environment that was created by the methane steam reforming reaction was responsible for reducing the char yield. The overall bio-oil yield was lower than that for cellulose, and it also was observed the yield decreased that when the catalyst was used. In addition, the increase in the gaseous fraction when the catalyst was used implied that there was a significant yield of non-condensable gases, such as CO and CO_2, as a result of the deoxygenation reaction.

The HHV of bio-oil increased with the upgrading process, and the highest value, i.e., 36,532.81 kJ/kg, occurred when methane was coupled with the Ni/ZSM-5 catalyst. . Figure 35 presents the elemental composition of bio-oil, showing an increase in carbon content and a decrease in oxygen content with upgrading. Sorghum biomass has about 0.22% nitrogen and about 0.08% sulfur. Nitrogen and sulfur levels were shown to have increased in Figure 35, indicating that the deoxygenation process did not remove any N or S from the bio-oil.

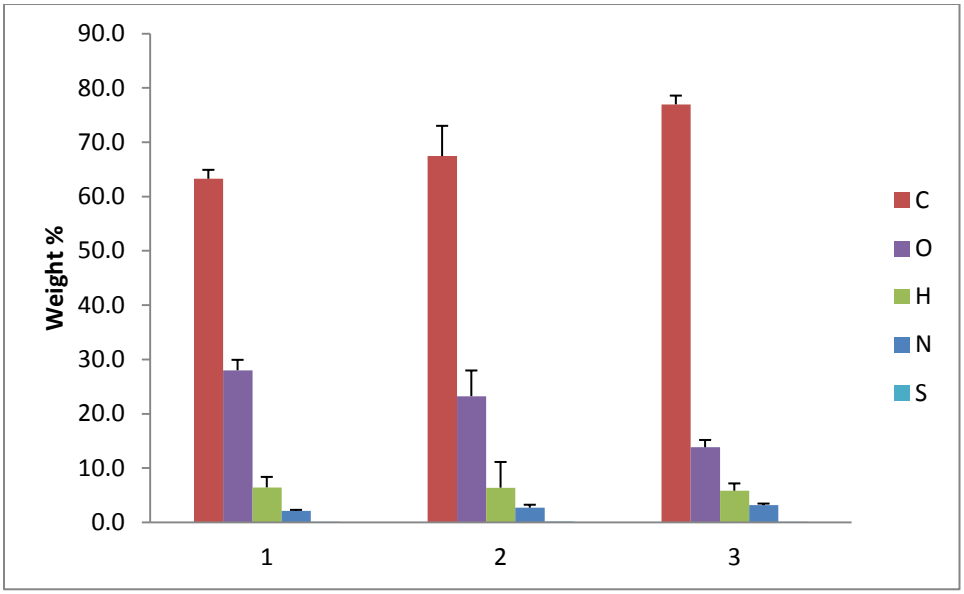

Figure 35. Elemental composition of bio-oil produced from sorghum: 1) raw bio-oil; 2) bio-oil from catalytic pyrolysis; 3)bio-oil from catalytic pyrolysis in the presence of methane (n=3, α=0.05)

Cost of producing bio-oil

Catalytically-treated, crude bio-oil costs were estimated by considering a plant that handles biomass at the rate of 100 metric tons/day. The batch process that was used for this study was very inefficient for large scale bio-oil production due to the slow heating rate of the batch reactor. In order to achieve higher bio-oil yields, the reactor system should be changed to a continuous system with a short resident time. Both processes were considered for the purposes of comparing costs. For the cost calculation for the batch process, the bio-oil yield was assumed to be 1.2%, and it was assumed to be 66% for the continuous fast pyrolysis process. It was assumed that the capital costs of the plant were paid in full at the beginning with no interest payments to be made. The costs of nitrogen and methane were estimated according to Airgas' standard industrial pricing.

The costs of the catalysts were estimated to be $100/kg. According to a report published by Texas A&M's Agrilife Extension Service, the production cost of sorghum is about $24.58/wet ton [125]. In Texas, the average selling price of electricity for the industrial sector was $0.06/kWh during the first quarter of 2014. The plant was assumed to operate 24 hr/day for 330 days/year. The capital cost for the slow pyrolysis plant was taken as $6,600,000 while the fast pyrolysis plant was estimated to cost 20% more than the slow pyrolysis plant.

Table 14. Costs for the production of bio-oil using the slow pyrolysis and fast pyrolysis processes

Item	Slow pyrolysis	Fast pyrolysis
Biomass weight per year (US tons/year)	36376.23	36376.23
Capital cost	$6,600,000	$7,920,000.0
Cost of electricity	$0.06/kWh	$0.06/kWh
Feedstock Cost	$891,945	$891,945
Grinding Cost	$181,881	$181,881
Electricity for the processes	$909,088	$961,360
Nitrogen	$2,788.18	$2,788.18
Solvent and Catalyst	$15,124,903	$15,124,903
Methane	$35,688.69	$35,688.69
Labor - 10 employees	$487,500	$487,500
Maintenance	$660,000	$792,000
Potable water, heat exchanger water, sewage	$10,000	$10,000
Supplies and Services	$62,857	$62,857
Total annual operating cost	$18,366,651	$18,550,923
Gallons Produced	73,266	4,395,941
Dollars per Gallon	$250.69	$4.22

According to the cost calculation given in Table (14), bio-oil from the slow pyrolysis plant would cost about $250.69/gal, which is extremely expensive. The primary reason for this high cost is the low percentage yield that was used. The fast pyrolysis process had a significantly lower price of $4.22/gal. At this rate, a barrel of bio-oil would cost $132.93 which is still higher than the cost of a barrel of petroleum. In order to reduce the price of bio-oil, it is very critical to reduce the cost of the catalyst.

Specific conclusions

The possibility of using methane as a proton donor for the deoxygenation process was studied. The results clearly indicated that the presence of methane improved the quality of the bio-oil. The low yield of bio-oil from cellulose and sorghum was due to the slow pyrolysis that occurred in the batch reactor. Low yield and the catalyst cost contributed to higher prices of bio-oil from sorghum. By using the fast the pyrolysis process instead, the cost per gallon of bio-oil was reduced to $4.22. Further reduction in the price is necessary to compete with existing petroleum crude. In order to further reduce the cost of bio-oil, the costs of the catalysts must be decreased significantly.

CHAPTER VIII

CONCLUSIONS

The status quo of lignocellulosic biofuel production using thermochemical processes is not favorable for the longevity of the biofuel industry. Almost the entire biofuel industry survives only because it receives government subsidies. The underlying reason for the industry's need to depend on government subsidies is its unfavorable process economics. To compete with the petrochemical industry, processes that can reduce the costs associated with converting biomass to biofuels must be developed.

In this study, we presented a novel chemical process that can be used with the thermochemical process. The results that were achieved are unprecedented in research related to the conversion of biomass to hydrocarbon biofuels. The use of hydrogen-rich, naturally-occurring alkanes as hydrogen carriers and the use of these alkanes over bi-functional, shape-selective zeolite catalysts constituted a significant departure from existing approaches and have the potential to have a transformative impact on the hydrodeoxygenation of biomass.

In the first part of the study, it was proved that it is possible to remove oxygen from oxygenates by incorporating methane as the proton donor for the deoxygenation reaction. This conclusion was reached by co-processing methane with glucose pyrolysis vapor, which contains various oxygenated compounds. By using isotope-labeled glucose and methane, it was proved that three reactions involving methane and glucose pyrolysis vapor likely take place depending on the type of the catalyst used. Specifically,

Ga/ZSM-5, Mo/ZSM-5, and Pt/ZSM-5 catalysts promote the direct methane aromatization reaction. The coupling of steam reforming with the deoxygenation reaction occurred in the presence of Ni/ZSM-5 and Pt/ZSM-5 catalysts. It also was proved that, in the presence of catalysts, such as Ga/ZSM-5 and Mo/ZSM-5, carbon and hydrogen participate in a hydrocarbon pool mechanism to form hydrocarbons.

A system with 11 species was considered in the thermodynamic equilibrium model. The analyses indicated that aromatic fractions do not appear in significant quantities in the equilibrium mixture. According to the calculations, the system had a high tendency to move toward thermodynamically-stable species, such as CH_4, CO_2, H_2O, CO, H_2, and C, at thermal equilibrium. The results of the analysis indicated that the actual results followed the thermodynamic predictions fairly closely for the trends of the gaseous species of CH_4 and CO_2, while the CO results that were obtained did not follow the thermodynamic predictions. Unfortunately, the thermodynamic model did not accurately predict the formation of aromatic products. It was observed that the inclusion of stable species in the model always forced the system to converge toward species that were more thermodynamically stable. One suggestion to circumvent this issue is to use a reaction mechanism that has several different intermediate steps and is subject to equilibrium using the Gibbs free energy minimization method. As a result of this analysis, we conjectured that the aromatic products in the pyrolysis experiment were produced before the system actually reached thermodynamic equilibrium. Therefore, these aromatic products must be treated as intermediates that eventually will be

converted to more thermodynamically stable species as the system approaches equilibrium.

The catalyst screening study focused on understanding the effect of different metals and metal oxides on the methane coupled deoxygenation process. It was concluded that metals and metal oxides had significant impacts on furan conversion. The results showed that Ga, Mo, and Cr, which exist in oxide forms, decreased the furan conversion when the impregnation level was increased from 1 to 5%. A plausible explanation for this is that the higher metal loading resulted in great pore blocking, thereby reducing the conversion. However, the results obtained when Pt- and Ni-loaded ZSM-5 catalysts were used were counter to this observation, since they produced higher conversions at higher metal loadings. The highest selectivity of 5.93% for BTEX was observed for Ga_2O_3 at 5% loading. Of the two metals tested, 1% Pt showed the highest selectivity of 4.41% for BTEX when methane was present. However, Ni produced a higher conversion than Pt in the presence of methane, likely due to the better performance of Ni in the steam reforming reaction. Since the objective of this process was to couple steam reforming with the deoxygenation process, Ni can be recommended as the metal for the reaction.

According to the kinetics study, the furan conversion rate was first order with respect to methane and second order with respect to furan concentration. The kinetic parameters of activation energy pre-exponential factor were 54.108 kJ.mol and 4.53 x 10^4 $l^2m^{-2}s^{-1}$, respectively. The carbon selectivities for the products such as benzene, toluene, ethyl benzene, and xylene, were affected significantly by the temperature.

Higher temperatures favored the selectivity for benzene, while low temperatures favored the selectivity for ethyl benzene and xylene. Benzene reported the highest carbon selectivity of 2.54% at WHSV = 42.69 h^{-1} at700 ^{o}C.

We conducted a study of catalyst deactivation, which provided insight into catalyst poisoning, fouling, and sintering. Poisoning and thermal degradation generally are irreversible, while fouling by solid carbon or polyaromatics can be reversed easily. Carbon deposition and coking can be minimized by improving the mass transport in the catalyst bed. Sintering can be avoided by selecting low operating temperatures. The results indicated that the catalyst activity decreased significantly, and the catalyst had to be regenerated 40 min after the reaction started. At 500 ^{o}C, the catalyst activity can be restored back to the original level, but at temperatures above600 ^{o}C, the activity could not be fully restored due to sintering.

The possibility of using methane as a proton donor for the deoxygenation process was studied in a batch reactor with biomass. The analysis of bio-oil from two different feedstocks, i.e., cellulose and sorghum, clearly indicated that the presence of methane improved the quality of the bio-oil. The low yield of bio-oil from cellulose and sorghum was due to the slow pyrolysis that took place in the batch reactor. Low yield and the cost of the catalyst resulted in a much higher price for the bio-oil derived from sorghum. By using the fast pyrolysis process, the cost per gallon of bio-oil was reduced from $250.69 to $4.22. However, further reduction in the price is necessary if bio-oil is to compete with existing petroleum crude. In order to further reduce the cost of bio-oil, the cost of the catalyst must be decreased significantly.

This study shed elucidated some of the complexities of an important area in which a short-chain hydrocarbon can be used as a proton donor. No previous work has reported biomass deoxygenation coupled with the activation of hydrocarbons. Fundamental studies on the catalytic chemistry gave some insights into how C-H bond activation and deoxygenation work concurrently. This understanding allows us to focus on certain areas of the process for further improvement. Instead of metal impregnation, it is possible to incorporate metals into the structure of the zeolite cage (isomorphous substitution), which possibly could improve pore the restrictions that were encountered when the catalyst was impregnated with the metal. Further, it was observed that the catalyst support underwent thermal deactivation above 600 ^{o}C. To circumvent this issue, the reaction temperature should be lowered without compromising the reaction rates. However, methane does not provide much leeway in changing the temperature, because C-H bond activation requires a significant amount of energy. Therefore, it is important to assess hydrocarbons with more than one carbon, such as propane or butane. Testing natural gas instead of methane is another option that can be very attractive from the standpoint of reducing costs.

The batch reactor is not a good choice for large scale bio-oil production due to its poor bio-oil yields. To incorporate fast pyrolysis, the reactor system must be changed to either a fluidized bed reactor or a continuous auger-type reactor. As an additional improvement, the catalyst could be mixed with the biomass instead of placing it in a plug flow reactor. Having catalyst mixed with biomass would make it easier to regenerate with an auger-type reactor.

REFERENCES

1. Perlack, R. D., et al., *Biomass as feedstocks for a bioenergy and bioproducts industry: The technical feasibility of a billion-ton annual supply* 2005, Oak Ridge National Laboratory: Oak Ridge, Tennessee Available from: http://www.osti.gov/bridge.
2. Gosselink, J. W., *Pathways to a more sustainable production of energy: Sustainable hydrogen:a research objective for shell.* International Journal of Hydrogen Energy, 2002. **27**(12): p. 1125-1129.
3. Katzen, R. and D. J. Schell, *Lignocellulosic feedstock biorefinery: history and plant development for biomass hydrolysis*, in *Biorefineries-Industrial Processes and Products: Status Quo and Future Directions*, B. Kamm, P. R. Gruber and M. Kamm, Editors. 2006, Wiley-VCH Verlag GmbH & Co. KGaA.: Weinheim, Germany. p. 129-138.
4. Kamm, B. and M. Kamm, *Biorefinery -System.* Chemical and Biochemical Engineering Quarterly, 2004. **18**(1): p. 1-6.
5. Demirbas, A., *Biofuels sources, biofuel policy, biofuel economy and global biofuel projections.* Energy Conversion and Management, 2008. **49**(8): p. 2106–2116.
6. Demirbas, M. F. and M. Balat, *Recent advances on the production and utilization trend of bio-fuels: A global perspective.* Energy Conversion and Management, 2006. **47**(15): p. 2371-2381.

7. Janssen, F., *Catalysis for renewable energy and chemicals, the thermal conversion of biomass.* Environmental Catalysis, 1999. **1**: p. 15-36.

8. Yoshida, Y., et al., *Comprehensive comparison of e ciency and CO_2 emissions between biomass energy conversion technologies position of supercriticalwater gasification in biomass technologies.* Biomass and Bioenergy, 2003. **25**(3): p. 257-272.

9. Bridgwater, A. V., D. Meier and D. Radlein, *An overview of fast pyrolysis of biomass.* Organic Geochemistry, 1999. **30**(12): p. 1479-1493.

10. Hill, J., E. Nelson, D. Tilman, S. Polasky and D. Tiffany, *Environmental, economic, and energetic costs and benefits of biodiesel and ethanol biofuels.* Proceedings of the National Academy of Sciences of the United States of America, 2006. **103**(30): p. 11206-11210.

11. Zurer, P., *Biofuels reality check.* Chemical and Engineering News, 2006. **84**(30): p. 3.

12. Li, J., L. Wu and Z. Yang, *Analysis and upgrading of bio-petroleum from biomass by direct deoxy-liquefaction.* Journal of Analytical and Applied Pyrolysis, 2008. **81**(2): p. 199–204.

13. Hayes, D. J., *An examination of biorefining processes, catalysts and challenges.* Catalysis Today, 2009. **145** (2): p. 138-153.

14. Klerk, A. D., *Hydroprocessing peculiarities of Fischer-Tropsch syncrude.* Catalysis Today, 2008. **130**(2): p. 439-445.

15. Maitlis, P. M., *Fischer–Tropsch, organometallics, and other friends.* Journal of Organometallic Chemistry, 2004. **689**(24): p. 4366–4374.

16. Lamprecht, D., *Hydrogenation of Fischer-Tropsch synthetic crude.* Energy & Fuels, 2007. **21**(5): p. 2509-2513.

17. Lin, Y. C., J. Cho, G. A. Tompsett, P. R. Westmoreland and G. W. Huber, *Kinetics and mechanism of cellulose pyrolysis.* The Journal of Physical Chemistry C, 2009 **113**(46): p. 20097–20107.

18. Kleinert, M., J. R. Gasson and T. Barth, *Optimizing solvolysis conditions for integrated depolymerisation and hydrodeoxygenation of lignin to produce liquid biofuel.* Journal of Analytical and Applied Pyrolysis, 2009. **85**: p. 108–117.

19. Li, H., et al., *Liquefaction of rice straw in sub- and supercritical 1,4-dioxane-water mixture.* Fuel Processing Technology, 2009. **90**: p. 657–663.

20. Mullaney, H., I. H. Farag, C. E. LaClair and C. J. Barrett, *Technical, environmental and economic feasibility of Bio-Oil in New Hampshire's north country*. 2002, University of New Hampshire Available from: file:///D:/Research/Bio%20Oil%20program/Pyrolysis/Bio%20oil%20report.pdf.

21. Zhang, Q., J. Chang, T. Wang and Y. Xu, *Upgrading Bio-oil over different solid catalysts.* Energy & Fuels, 2006. **20**(6): p. 2717-2720.

22. Senneca, O., *Kinetics of pyrolysis, combustion and gasification of three biomass fuels.* Fuel Processing Technology, 2007. **88**(1): p. 87–97.

23. Adjaye, J. D., R. K. Sharma and N. N. Bakhshi, *Characterization and stability analysis of wood-derived bio-oil.* Fuel Processing Technology, 1992. **31**(3): p. 241-256.

24. Bridgwater, T., *Biomass for energy.* Journal of the Science of Food and Agriculture, 2006. **86**(12): p. 1755-1768.

25. Hoekstra, E., et al., *Fast pyrolysis of biomass in a fluidized bed reactor: In situ filtering of the vapors.* Industrial & Engineering Chemistry Research, 2009. **48**: p. 4744–4756.

26. Bridgwater, A. V., *Production of high grade fuels and chemicals from catalytic pyrolysis of biomass.* Catalysis Today, 1996. **29**(4): p. 285–295.

27. Elliott, D. C., *Historical developments in hydroprocessing bio-oils.* Energy & Fuels, 2007. **21**(3): p. 1792-1815.

28. Mohan, D., C. U. Pittman and P. H. Steele, *Pyrolysis of wood/biomass for bio-oil: A critical review* Energy & Fuels, 2006. **20**(3): p. 848-889.

29. Taner, F., A. Eratik and I. Ardic, *Identification of the compounds in the aqueous phases from liquefaction of lignocellulosics.* Fuel Processing Technology, 2004. **86**(4): p. 407-418.

30. Fernando, S., S. Adhikari, C. Chandrapal and N. Murali, *Biorefineries:Current status, challenges, and future direction.* Energy & Fuels, 2006. **20**(4): p. 1727-1737.

31. Adjaye, J. D. and N. N. Bakhshi, *Production of hydrocarbons by catalytic upgrading of a fast pyrolysis bio-oil. Part I: Conversion over various catalysts.* Fuel Processing Technology, 1995. **45**(3): p. 161-183.

32. Zhang, Q., J. Chang, T. Wang and Y. Xu, *Review of biomass pyrolysis oil properties and upgrading research.* Energy Conversion and Management, 2007. **48**(1): p. 87-92.

33. Radovanovic, M., R. H. Venderbosch, W. Prins and W. P. M. V. Swaaij, *Some remarks on the viscosity measurement of pyrolysis liquids.* Biomass and Bioenergy, 2000. **18**(3): p. 209-222.

34. Furimsky, E., *Catalytic hydrodeoxygenation.* Applied Catalysis A: General, 2000. **199**(2): p. 147–190.

35. Yang, Y. Q., C. T. Tye and K. J. Smith, *Influence of MoS_2 catalyst morphology on the hydrodeoxygenation of phenols.* Catalysis Communications, 2008. **9**(6): p. 1364–1368.

36. Kim, S. C. and F. E. Massoth, *Kinetics of the hydrodenitrogenation of Indole.* Industrial & Engineering Chemistry Research, 2000. **39**(6): p. 1705-1712.

37. Laurent, E. and B. Delmon, *Study of the hydrodeoxygenation of carbonyl, carboxylic and guaiacyl groups over sulfided $CoMo/\gamma$-Al_2O_3 and $NiMo/_g$-Al_2O_3 catalyst: II. Influence of water, ammonia and hydrogen sulfide.* Applied Catalysis A: General, 1994. **109**(1): p. 97-115.

38. Yakovlev, V. A., et al., *Development of new catalytic systems for upgraded bio-fuels production from bio-crude-oil and biodiesel.* Catalysis Today, 2009. **144**(3-4): p. 362.

39. Odebunmi, E. O. and D. F. Ollis, *Catalytic Hydrodeoxygenation: I. Conversions of o-, p-, and m-cresols.* Journal of Catalysis, 1983. **80**(1): p. 56-64.

40. Bejblova, M., P. Zamostny, L. Cerveny and J. Cejka, *Hydrodeoxygenation of benzophenone on Pd catalysts.* Applied Catalysis A: General, 2005. **296**(2): p. 169–175.

41. Elliott, D. C. and G. G. Neuenschwander, *Liquid fuels by low-severity hydrotreating of biocrude, developments in thermochemical biomass conversion*, ed. A. V. Bridgwater and D. G. B. Boocock. Vol. **1**. 1996, London: Blackie Academic & Professional. 621.

42. Senol, O. I., T. R. Viljava and A. O. I. Krause, *Hydrodeoxygenation of methyl esters on sulphided NiMo/γ-Al_2O_3 and CoMo/γ-Al_2O_3 catalysts.* Catalysis Today, 2005. **100**(3): p. 331-335.

43. Zhang, S. P., Y. J. Yan, Z. Ren and T. Li, *Study of hydrodeoxygenation of bio-oil from fast pyrolysis of biomass.* Energy Sources, 2003. **25**(1): p. 57-65.

44. Viljava, T. R., *From biomass to fuels: Hydrotreating of oxygencontaining feeds on a CoMo/Al_2O_3 hydrodesulfurization catalyst*, in *Department of Chemical Technology* 2001, Helsinki University of Technology: Espoo, Finland.

45. Samolada, M. C. and I. A. Vasalos, *Catalytic cracking of biomass flash pyrolysis liquids.* Developments in Thermochemical Biomass Conversion, 1997. **1**: p. 657-671.

46. Samolada, M. C. and I. A. Vasalos. *Production of transportation fuels by upgrading of biomass flash pyrolysis liquids via FCC technology*. in *Biomass for Energy and the Environment, Proceedings of the 9th European Bioenergy Conference,* . 1996. Copenhagen.

47. Maher, K. D. and D. C. Bressler, *Pyrolysis of triglyceride materials for the production of renewable fuels and chemicals.* Bioresource technology, 2007. **98**(12): p. 2351-2361.

48. Vitolo, S., B. Bresci, M. Seggiani and M. G. Gallo, *Catalytic upgrading of pyrolytic oils over HZSM-5 zeolite: behaviour of the catalyst when used in repeated upgrading-regenerating cycles.* Fuel, 2001. **80**(1): p. 17-26.

49. Wilson, N. G. and P. T. Williams, *Investigation into the potential of a novel superacid catalyst for the catalytic upgrading of pyrolytic bio-oil.* Int. J. Energy Res., 2003. **27**(2): p. 131-143.

50. Corma, A., G. W. Huber, L. Sauvanaud and P. O'Connor, *Processing biomass-derived oxygenates in the oil refinery: Catalytic cracking (FCC) reaction pathways and role of catalyst.* Journal of Catalysis, 2007. **247**(2): p. 307-327.

51. Senol, O. I., E. M. Ryymin, T. R. Viljava and A. O. I. Krause, *Effect of hydrogen sulphide on the hydrodeoxygenation of aromatic and aliphatic oxygenates on sulphided catalysts.* Journal of Molecular Catalysis A: Chemical, 2007. **277**(1): p. 107-112.

52. Elliott, D. C. and G. G. Neuenschwander, *Liquid fuels by low-severity hydrotreating of biocrude.* Development in Thermochemical Biomass Conversion, 1997. **1**: p. 611-621.

53. Elliott, D. C., et al., *Environmental impacts of thermochemical biomass conversion*. 1995, National Renewable Energy Laboratory: Golden, Colorado.

54. Fisk, C., et al. *Novel approaches to catalytic upgrading of bio-oil*. in *ASABE Annual International Meeting*. 2006. Portland, Oregon.

55. Laurent, E., R. Maggi and B. Delmon. *Partial and full hydrorefining of pyrolysis oils: Overview and feasibility assessment*. in *Biomass for Energy, Environment, Agriculture and Industry, Proceedings of the 8th European Biomass Conference* 1994. Vienna: Elsevier.

56. Nielsen, J. R. R. and T. R. Nielsen, *Large-scale hydrogen production.* CATTECH, 2002. **6**(4): p. 150-159.

57. Pena, M. A., J. P. Gomez and J. L. G. Fierro, *New catalytic routes for syngas and hydrogen production.* Applied Catalysis, A: General, 1996. **144**(1-2): p. 7-57.

58. Ritter, J. A. and A. D. Ebner, *State-of-the-art adsorption and membrane separation processes for hydrogen production in the chemical and petrochemical industries.* . Separation Science and Technology, 2007. **42**(6): p. 1123-1193.

59. Shekhawat, D., D. A. Berry, T. H. Gardner and J. J. Spivey, *Catalytic reforming of liquid hydrocarbon fuels for fuel cell applications* Catalysis, 2006. **19**: p. 184-254.

60. Farrauto, R., et al., *New material needs for hydrocarbon fuel processing: Generating hydrogen for the PEM fuel cell.* Annu. Rev. Mater. Res., 2003. **33**: p. 1–27.

61. Liu, S., K. Takahashi, K. Uematsu and M. Ayabe, *Hydrogen production by oxidative methanol reforming on Pd/ZnO.* Applied Catalysis A: General, 2005. **283**(2): p. 125-135.

62. Choudhary, V. R. and S. A. R. Mulla, *Coupling of thermal cracking with noncatalytic oxidative conversion of ethane to ethylene* AIChE Journal, 1997. **43**(6): p. 1545-1550.

63. Choudhary, V. R., S. A. R. Mulla and V. H. Rane, *Coupling of exothermic and endothermic reactions in oxidative conversion of ethane to ethylene over alkaline earth promoted La_2O_3 catalysts in presence of limited O_2.* Applied Energy, 2000. **66**(1): p. 51-62.

64. Towler, G. and S. Lynn, *Novel application of reaction coupling: use of carbon dioxide to shift the equilibrium of dehydrogenation reactions.* Chemical Engineering Science, 1994. **49**(6): p. 2585-2591.

65. Zhao, T. J., et al., *Rational design of the carbon nanofiber catalysts for oxidative dehydrogenation of ethylbenzene.* Applied Catalysis, A: General, 2007. **323**(30): p. 135-146.

66. Wang, S. and Z. H. Zhu, *Catalytic conversion of alkanes to olefins by carbon dioxide oxidative dehydrogenation:A review.* Energy & Fuels, 2004. **18**(4): p. 1126-1139.

67. Sun, A., Z. Qin and J. Wang, *Reaction coupling of ethylbenzene dehydrogenation with nitrobenzene hydrogenation.* Catalysis Letters, 2002. **79**(4): p. 33-37.

68. Sitthisa, S. and D. E. Resasco, *Hydrodeoxygenation of furfural over supported metal catalysts: A comparative study of Cu, Pd and Ni.* Catalysis Letters, 2011. **141**(6): p. 784-791.

69. Qiu, P., J. Lunsford and M. Rosynek, *Characterization of Ga/ZSM-5 for the catalytic aromatization of dilute ethylene streams.* Catalysis Letters, 1998. **52**(1): p. 37-42.

70. Xu, Y., S. Liu, L. Wang, M. Xie and X. Guo, *Methane activation without using oxidants over Mo/ZSM-5 zeolite catalyst.* Catalysis Letters 30 (1995) 135-149, 1995. **30**(1-4): p. 135-149.

71. Thring, R. W., S. P. R. Katikaneni and N. N. Bakhshi, *The production of gasoline range hydrocarbons from Alcell-R lignin using HZSM-5 catalyst.* Fuel Processing Technology, 2000. **62**(1): p. 17-30.

72. Hou, K. and R. Hughes, *The kinetics of methane steam reforming over a Ni/α-Al_2O_3 catalyst.* Chemical Engineering Journal, 2001. **82**(3): p. 311-328.

73. McGrath, T. E., W. G. Chan and M. R. Hajaligol, *Low temperature mechanism for the formation of polycyclic aromatic hydrocarbons from the pyrolysis of cellulose.* Journal of Analytical and Applied Pyrolysis, 2003. **66**(2): p. 51-70.

74. Carlson, T. R., J. Jae, Y. C. Lin, G. A. Tompsett and G. W. Huber, *Catalytic fast pyrolysis of glucose with HZSM-5: The combined homogeneous and heterogeneous reactions.* Journal of Catalysis, 2010. **270**(1): p. 110–124.

75. Paine, J. B., Y. B. Pithawalla and J. D. Naworal, *Carbohydrate pyrolysis mechanisms from isotopic labeling: Part 2. The pyrolysis of D-glucose: General disconnective analysis and the formation of C_1 and C_2 carbonyl compounds by electrocyclic fragmentation mechanisms.* Journal of Analytical and Applied Pyrolysis, 2008. **82**(1): p. 10-41.

76. Silva, A. L. d., C. l. d. F. Malfatti and I. L. Muller, *Thermodynamic analysis of ethanol steam reforming using Gibbs energy minimization method: A detailed study of the conditions of carbon deposition.* International Journal of Hydrogen Chemistry, 2009. **34** (10): p. 4321-4330.

77. Baratieri, M., P. Baggioa, L. Fioria and M. Grigiante, *Biomass as an energy source: Thermodynamic constraints on the performance of the conversion process* Bioresource Technology, 2008. **99**(15): p. 7063-7077.

78. Burcat, A. and B. Ruscic, *Third millennium ideal gas and condensed phase: Thermochemical database for combustion with updates from active thermochemical tables*. 2005, Argonne National Laboratory: Argonne, Illinois Available from: http://www.osti.gov/bridge.

79. Gunawardena, D. A. and S. D. Fernando, *Thermal conversion of glucose to aromatic hydrocarbons via pressurized secondary pyrolysis.* Bioresource Technology, 2011. **102**(21): p. 10089-10093.

80. Adhikaria, S., et al., *A thermodynamic analysis of hydrogen production by steam reforming of glycerol.* International Journal of Hydrogen Energy, 2007. **32**(14): p. 2875 – 2880.

81. Amin, N. A. S. and S. E. Peng, *A thermodynamic equilibrium analysis on oxidation of Methane to higher hydrocarbons.* Pertanika Journal of Science and Technology, 2009. **17**(2): p. 363 – 370.

82. Grandmaison, J. L., P. D. Chantal and S. C. Kaliaguine, *Conversion of furanic compounds over H-ZSM-5 zeolite.* Fuel, 1990. **69**(8): p. 1058–1061.

83. Choudhary, T. V., E. Aksoylu and D. W. Goodman, *Nonoxidative activation of methane.* Catalysis Reveiws, 2003. **45**(1): p. 151–203.

84. Gueret, C., M. Daroux and F. Billaudi, *Methane pyrolysis: thermodynamics.* Chemcol Engineermg Science, 1997. **52**(5): p. 815-827.

85. Amariglio, H., J. Saint-Justb and A. Amariglio, *Homologation of methane under non-oxidative conditions.* Fuel Processing Technology, 1995. **42**(2): p. 232391.

86. Wang, D., J. H. Lunsford and M. P. Rosynek, *Characterization of a Mo/ZSM-5 Catalyst for the conversion of methane to benzene.* Journal of Catalysis, 1997. **169**(1): p. 347–358.

87. Yaws, C. L., *Yaws' handbook of thermodynamic properties for hydrocarbons and chemicals*. 2009, Knovel online library Available from: http://app.knovel.com/web/toc.v/cid:kpYHTPHC09.

88. Cheng, Y. T. and G. W. Huber, *Chemistry of furan conversion into aromatics and olefins over HZSM-5: A model biomass conversion reaction.* ACS Catalalysis, 2011. **1**(6): p. 611–628.

89. Karushaar, B., H. Kompa, H. Schrubbers and G. Schulz-Ekloff, *Hydrodeoxygenation of furan on H-ZSM-5 and Pt-ZSM-5.* Acta Physica Et Chemica, 1985. **31**(2): p. 581-587.

90. Ismagilov, Z. R., E. V. Matus and L. T. Tsikoza, *Direct conversion of methane on Mo/ZSM-5 catalysts to produce benzene and hydrogen: achievements and perspectives.* Energy & Environmental Science, 2008. **1**(5): p. 526-541.

91. Lukyanov, D. B. and T. Vazhnova, *Selective and stable benzene alkylation with methane into toluene over Pt/H-MFI bifunctional catalyst.* Journal of Molecular Catalysis A: Chemical, 2009. **305**(2): p. 95–99.

92. Bond, G. C., G. Webb and J. R. H. Ross, *Metal catalysed methanation and steam reforming*, in *Catalysis*, G. C. Bond and G. Webb, Editors. 1985, Royal Society of Chemistry: Oxford, London. p. 1-45.

93. Amin, N. A. S. and D. D. Anggoro, *Characterization and activity of Cr, Cu and Ga modied ZSM-5 for direct conversion of methane to liquid hydrocarbons.* Journal of Natural Gas Chemistry, 2003. **12**(2): p. 123 -134.

94. Cheng, Y. T., J. Jae, J. Shi, W. Fan and G. W. Huber, *Production of renewable aromatic compounds by catalytic fast pyrolysis of lignocellulosic biomass with bifunctional Ga/ZSM-5 catalysts.* Angewandte Chemie, 2012. **124**(6): p. 1416–1419.

95. Choudhary, V. R., K. C. Mondal and S. A. R. Mulla, *Simultaneous conversion of methane and methanol into gasoline over bifunctional Ga-, Zn-, In-, and Mo-modified ZSM-5 Zeolites.* Angewandte Chemie, 2005. **117**(28): p. 4455–4459.

96. Xu, B. J., B. Zheng, W. M. Hua, Y. H. Yue and Z. Gao. *High Si/Al ratio HZSM-5 supported Ga_2O_3: a highly stable catalyst for dehydrogenation of propane to propene in the presence of CO_2.* in *Zeolites to Porous MOF Materials - The 40th Anniversary of International Zeolite Conference*. 2007: Elsevier.

97. Wang, L., et al., *Dehydrogenation and aromatization of methane under non-oxidizing conditions.* Catalysis Letters, 1993. **21**(1-2): p. 35-41.

98. Mimura, N., M. Okamoto, H. Yamashita, S. T. Oyama and K. Murata, *Oxidative dehydrogenation of ethane over Cr/ZSM-5 catalysts using CO_2 as an oxidant.* Journal of Physical Chemistry B, 2006. **110**(43): p. 21764-21770.

99. Weckhuysen, B. M., D. Wang, M. P. Rosynek and J. H. Lunsford, *Conversion of methane to benzene over transition metal ion ZSM-5 Zeolites I. Catalytic characterization.* Journal of Catalysis, 1998. **175**(2): p. 338–346.

100. Zhu, T., et al., *Microkinetics of steam methane reforming on platinum and rhodium metal surfaces.* Journal of Catalysis, 2013. **297**: p. 227-235.

101. Grenoble, D. C., M. M. Estadt and D. F. Ollis, *The chemistry and catalysis of the water gas shift reaction: 1. The kinetics over supported metal catalysts.* Journal of Catalysis, 1981. **67**(1): p. 90-102.

102. Beurden, P. V., *On the catalytic aspects of steam-methane reforming*. 2004, Energy research centre of the Netherlands. p. 1-27 Available from: https://www.ecn.nl/publications/ECN-I--04-003.

103. Chorkendorff, I. and J. W. Niemantsverdriet, *Concepts of modern catalysis and kinetics*. 2007, Weinheim, Germany: Wiley-VCH Verlag GmbH & Co. KGaA. 477.

104. Zhai, X., S. Ding, Z. Liu, Y. Jin and Y. Cheng, *Catalytic performance of Ni catalysts for steam reforming of methane at high space velocity.* International Journal of Hydrogen Energy, 2011. **36**(1): p. 482–489.

105. Froment, G. F., K. B. Bischoff and J. D. Wilde, *Chemical reactor analysis and design*. 3 ed. 2008, New Jersey, USA: John Wiley & Sons, Inc. 837.

106. Zeppieria, M., P. L. Villab, N. Verdonea, M. Scarsellaa and P. D. Filippisa, *Kinetic of methane steam reforming reaction over nickel- and rhodium-based catalysts.* Applied Catalysis A: General, 2010. **387**(2): p. 147–154.

107. Xu, J. and G. F. Froment, *Methane steam reforming, methanation and water-gas shift: I. Intrinsic kinetics.* AIChE Journal, 1989. **35**(1): p. 88–96.

108. Nielsen, J. R. R., *Production of synthesis gas.* Catalysis Today, 1993. **18**(4): p. 305-324.

109. Wei, J. and E. Iglesia, *Mechanism and site requirements for activation and chemical conversion of methane on supported Pt clusters and turnover rate comparisons among noble metals.* The Journal of Physical Chemistry B, 2004. **108**(13): p. 4094–4103.

110. Hoang, D. L., S. H. Chan and O. L. Ding, *Kinetic and modelling study of methane steam reforming over sulfide nickel catalyst on a gamma alumina support.* Chemical Engineering Journal, 2005. **112**(3): p. 1-11.

111. Furimsky, E., *The mechanism of catalytic hydrodeoxygenation of furan.* Applied Catalysis, 1983. **6**(2): p. 159–164.

112. Horne, P. A. and P. T. Williams, *The effect of zeolite ZSM-5 catalyst deactivation during the upgrading of biomass-derived pyrolysis vapours.* Journal of Analytical and Applied Pyroylsis, 1995. **34** (1): p. 65-85.

113. Aguayo, A. T., A. G. Gayubo, J. M. Ortega, M. Olazar and J. Bilbao, *Catalyst deactivation by coking in the MTG process in fixed and fluidized bed reactors.* Catalysis Today, 1997. **37**(3): p. 239-248.

114. Forzatti, P. and L. Lietti, *Catalyst deactivation.* Catalysis Today, 1999. **52**(2): p. 165-181.

115. Bhatia, S., *Zeolite Catalysts: principles and applications*. 1989, Florida, USA: CRC Press 304.

116. Guisnet, M. and F. R. Ribeiro, *Deactivation and regeneration of solid catalysts*. Catalytic Science Series, ed. Graham J. Hutchings. Vol. **9**. 2011, London, England: Imperial College Press. 335.

117. Bartholomew, C. H., *Mechanisms of catalyst deactivation.* Applied Catalysis A: General, 2001. **212**(1): p. 17–60.

118. Gunawardena, D. A. and S. D. Fernando, *Methods and Applications of Deoxygenation for the Conversion of Biomass to Petrochemical Products*, in *Biomass Now - Cultivation and Utilization*, M. D. Matovic, Editor. 2013, InTech: Rijeka, Croatia. p. 277-298.

119. Mullen, C. A., A. A. Boateng and N. M. Goldberg, *Production of deoxygenated biomass fast pyrolysis oils via product gas recycling.* Energy & Fuels, 2013. **27**(7): p. 3867-3874.

120. Overend, R. P., T. A. Milne and L. K. Mudge, *Fundamentals of thermochemical biomass conversion*. 1985, New York, USA: Elsevier Applied Science Publishers.

121. Zhu, X. F. and Q. Lu, *Production of chemicals from selective fast pyrolysis of biomass*, in *Biomass*, M. Ndombo and B. Momba, Editors. 2010, InTech: Rijeka, Croatia. p. 147-164.

122. Ko, C. H., et al., *Upgrading of biofuel by the catalytic deoxygenation of biomass.* Korean Journal of Chemical Engineering, 2012. **29**(12): p. 1657-1665.

123. Cordero, T., F. Marquez, J. Rodriguez-Mirasol and J. J. Rodriguez, *Predicting heating values of lignocellulosics and carbonaceous materials from proximate analysis.* Fuel, 2001. **80**(11): p. 1567-1571.

124. Mullen, C. A., G. D. Strahan and A. A. Boateng, *Characterization of various fast-pyrolysis bio-oils by NMR spectroscopy.* Energy & Fuels, 2009. **23**(5): p. 2707-2718.

125. Amosson, S., J. Girase, B. Bean, W. Rooney and J. Becker, *Economic analysis of Sweet Sorghum for biofuels production in the Texas high plains*. 2011, Texas Agriculture Experimental Station: Amarillo, Texas. Available from: http://amarillo.tamu.edu/amarillo-center-programs/agronomy/bioenergy-sorghum/.